NASA/TM—2009–000000

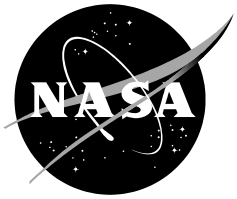

Mitigation of EMU Glove Cut Hazard by MMOD Impact Craters on Exposed ISS Handrails

Shannon Ryan
Lunar and Planetary Institute
Johnson Space Center, Houston, Texas

Eric L. Christiansen
Johnson Space Center, Houston, Texas

April 2009

NASA STI Program ... in Profile

Since its founding, NASA has been dedicated to the advancement of aeronautics and space science. The NASA scientific and technical information (STI) program plays a key part in helping NASA maintain this important role.

The NASA STI program operates under the auspices of the Agency Chief Information Officer. It collects, organizes, provides for archiving, and disseminates NASA's STI. The NASA STI program provides access to the NASA Aeronautics and Space Database and its public interface, the NASA Technical Report Server, thus providing one of the largest collections of aeronautical and space science STI in the world. Results are published in both non-NASA channels and by NASA in the NASA STI Report Series, which includes the following report types:

- TECHNICAL PUBLICATION. Reports of completed research or a major significant phase of research that present the results of NASA Programs and include extensive data or theoretical analysis. Includes compilations of significant scientific and technical data and information deemed to be of continuing reference value. NASA counterpart of peer-reviewed formal professional papers but has less stringent limitations on manuscript length and extent of graphic presentations.

- TECHNICAL MEMORANDUM. Scientific and technical findings that are preliminary or of specialized interest, e.g., quick release reports, working papers, and bibliographies that contain minimal annotation. Does not contain extensive analysis.

- CONTRACTOR REPORT. Scientific and technical findings by NASA-sponsored contractors and grantees.

- CONFERENCE PUBLICATION. Collected papers from scientific and technical conferences, symposia, seminars, or other meetings sponsored or co-sponsored by NASA.

- SPECIAL PUBLICATION. Scientific, technical, or historical information from NASA programs, projects, and missions, often concerned with subjects having substantial public interest.

- TECHNICAL TRANSLATION. English-language translations of foreign scientific and technical material pertinent to NASA's mission.

Specialized services also include creating custom thesauri, building customized databases, and organizing and publishing research results.

For more information about the NASA STI program, see the following:

- Access the NASA STI program home page at *http://www.sti.nasa.gov*

- E-mail your question via the Internet to help@sti.nasa.gov

- Fax your question to the NASA STI Help Desk at 443-757-5803

- Phone the NASA STI Help Desk at 443-757-5802

- Write to:
  NASA STI Help Desk
  NASA Center for AeroSpace Information
  7115 Standard Drive
  Hanover, MD 21076-1320

NASA/TM—2009–000000

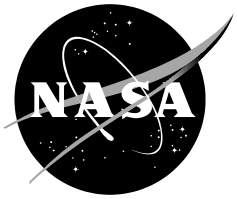

Mitigation of EMU Glove Cut Hazard by MMOD Impact Craters on Exposed ISS Handrails

Shannon Ryan
Lunar and Planetary Institute
Johnson Space Center, Houston, Texas

Eric L. Christiansen
Johnson Space Center, Houston, Texas

National Aeronautics and
Space Administration

Johnson Space Center
Houston, TX 77058

April 2009

Acknowledgments

All testing was performed at NASA JSC White Sands Test Facility in Las Cruces New Mexico.

Available from:

NASA Center for AeroSpace Information
7115 Standard Drive
Hanover, MD 21076-1320
443-757-5802

This report is also available in electronic form at

http://

Summary

Recent cut damages to crewmember extravehicular mobility unit (EMU) gloves during extravehicular activity (EVA) onboard the International Space Station (ISS) has been found to result from contact with sharp edges or pinch points rather than general wear or abrasion. One possible source of cut-hazards are protruding sharp edged crater lips from impact of micrometeoroid and orbital debris (MMOD) particles on external metallic handrails along EVA translation paths. During impact of MMOD particles at hypervelocity an evacuation flow develops behind the shock wave, resulting in the formation of crater lips that can protrude above the target surface. In this study, two methods were evaluated to limit EMU glove cut-hazards due to MMOD impact craters. In the first phase, four flexible overwrap configurations are evaluated: a felt-reusable surface insulation (FRSI), polyurethane polyether foam with beta-cloth cover, double-layer polyurethane polyether foam with beta-cloth cover, and multi-layer beta-cloth with intermediate Dacron netting spacers. These overwraps are suitable for retrofitting ground equipment that has yet to be flown, and are not intended to protect the handrail from impact of MMOD particles, rather to act as a spacer between hazardous impact profiles and crewmember gloves. At the impact conditions considered, all four overwrap configurations evaluated were effective in limiting contact between EMU gloves and impact crater profiles. The multi-layer beta-cloth configuration was the most effective in reducing the height of potentially hazardous profiles in handrail-representative targets. In the second phase of the study, four material alternatives to current aluminum and stainless steel alloys were evaluated: a metal matrix composite, carbon fiber reinforced plastic (CFRP), fiberglass, and a fiber metal laminate. Alternative material handrails are intended to prevent the formation of hazardous damage profiles during MMOD impact and are suitable for flight hardware yet to be constructed. Of the four materials evaluated, only the fiberglass formed a less hazardous damage profile than the baseline metallic target. Although the CFRP laminate did not form any noticeable crater lip, brittle protruding fibers are considered a puncture risk. In parallel with EMU glove redesign efforts, modifications to metallic ISS handrails such as those evaluated in this study provide the means to significantly reduce cut-hazards from MMOD impact craters.

Table of Contents

List of Figures

List of Tables

Glossary of Terms and Abbreviations

Al	Aluminum
BC	Beta-cloth
CFRP	Carbon Fiber Reinforced Plastic
CRV	Crew Return Vehicle
DROCF	Double layer Reticulated Open Cell Foam
EMU	Extravehicular Mobility Unit
EVA	Extravehicular Activity
FML	Fiber Metal Laminate
FRSI	Felt Reusable Surface Insulation
HITF	Hypervelocity Impact Technology Facility
HVI	Hypervelocity Impact
ISS	International Space Station
JSC	Johnson Space Center
MLI	Multi Layer Insulation
MMC	Metal Matrix Composite
MMOD	Micrometeoroid and Orbital Debris
n.a.	not applicable
NASA	National Aeronautics and Space Administration
NIST	National Institute of Standards and Technology
NTA	Nitrogen Tank Assembly
OCF	Open Cell Foam
OMS	Orbiter Maneuvering System
PPI	Pores Per Inch (linear)
RTV	Room Temperature Vulcanizing
SASA	S-band Antenna Structural Assembly
STS	Space Transportation System
TPS	Thermal Protection System

Notation

b_{max}	Maximum height of rear surface bulge
d_b	Bulge diameter (cm)
d_c	Crater diameter (cm)
d_h	Clear hole diameter (cm)
D_{max}	Maximum extension of damage (cm)
L_c	Length of longest crack (cm)
l_{max}	Maximum height of crater lip (cm)
p_{max}	Maximum crater depth (cm)
u.d.	Uni-directional
V_c	Crater volume (cm^3)
V_f	Fiber content by volume (%)

Subscripts:

1	Horizontal measurement
2	Vertical measurement
f	Front
r	Rear

Introduction

During post-flight processing of STS-116, damage to crewmember Robert Curbeam's Phase VI Glove Thermal Micrometeoroid Garment was discovered (shown in Figure 1). This damage consisted of: loss of RTV-157 palm pads on the thumb area on the right glove and a 0.75 inch cut in the Vectran adjacent to the seam and thumb pad (single event cut), constituting the worst glove damage ever recorded in "the history of going EVA for the U.S. program" [1] . The underlying bladder and restraint were found not be damaged.

Figure 1: Damge to crewmember Curbeam's Phase VI glove following EVA 3 of STS-116.

Evaluation of glove damage showed that the outer Vectran fibers were sliced as a result of contact with a sharp edge or pinch point rather than general wear or abrasion (commonly observed on the RTV pads). Damage to gloves was also noted on STS-118 [2] and STS-120 [3].

One potential source of Extravehicular Mobility Unit (EMU) glove damage are sharp crater lips on external ISS handrails. Hundreds of handrails are installed on the external surface of the ISS and are therefore subject to impact from micrometeoroid and orbital debris (MMOD) particles. Returned flight hardware has demonstrated the susceptibility of these structures to regular MMOD impacts, examples of which are shown in Figure 2 (ISS Airlock, S-band Antenna Structural Assembly (SASA)) and Figure 3 (Nitrogen Tank Assembly (NTA)).

Figure 2: Damage to returned handrail surfaces by possible MMOD impacts. Left: ISS Airlock handrail (~1.8 mm outer diameter crater); Right: SASA handrail (~0.5 mm diameter crater).

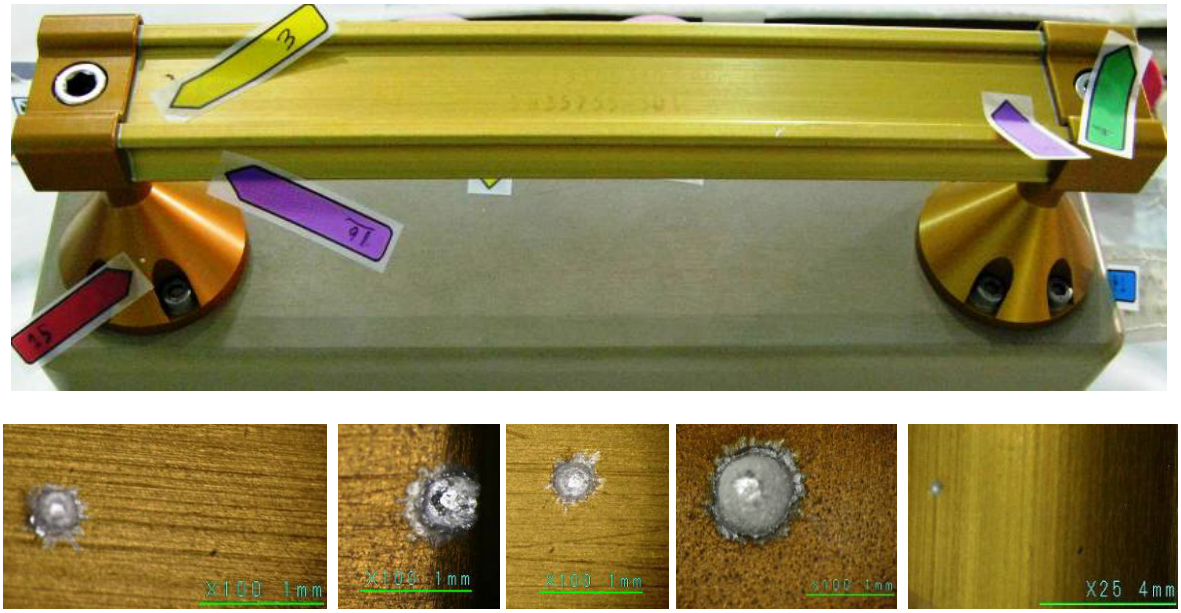

Figure 3: MMOD impacts on the returned NTA handrail. Top: Location of impacts; Below: Close-up of impact craters (from left-to-right: impacts 3, 4, 5, 15, 16).

Redesign efforts are currently underway to increase the resilience of EMU gloves. For example, during STS-124 a modified EMU glove was used that incorperated Vectran TurtleSkin© patches on areas of high wear (lower part of thumb and upper part of index finger). TurtleSkin is a protective fabric material commonly used in protective vests for knife protection given its extremely tight weave, providing superior protection against cuts and penetration than common woven fabrics. The modified glove is shown in Figure 4. Preliminary analysis of glove damage suggested that the modification was successful in reducing glove damage.

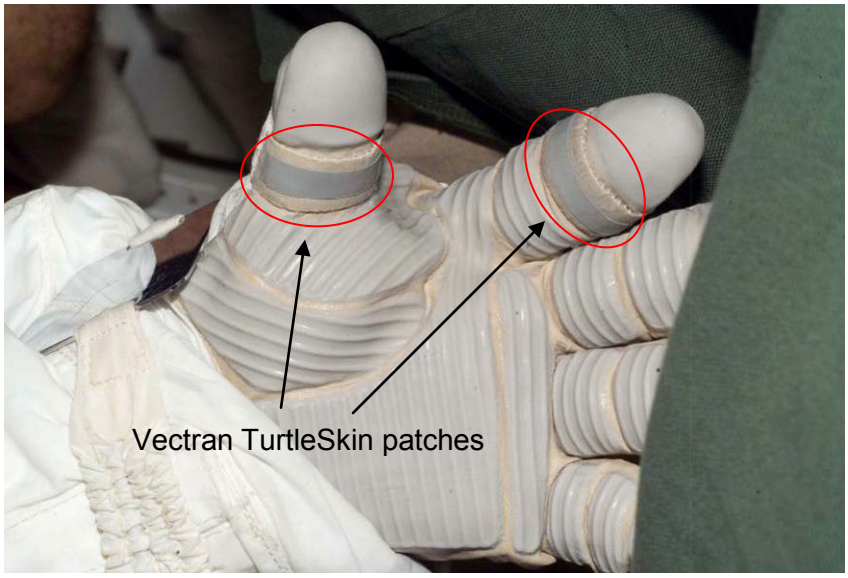

Figure 4: Vectran TurtleSkin reinforcement patches added to index finger and thumb of the Phase VI EMU glove for STS-124.

In addition to glove modifications, it is useful to evaluate handrail structures and materials in order to reduce sources of MMOD damages that represent potential cut hazards for EVA crew. Two alternate means of reducing MMOD impact crater sites as EMU glove cut hazards are evaluated in this study:

- Flexible overwraps that can be added to existing handrails (such as ground equipment that is yet to be flown) and will effectively act as padding, limiting the contact between sharp crater lips and EVA crew gloves, and;
- Alternative materials for ISS handrails that result in MMOD impact craters that minimize the potential cut hazard to EMU gloves.

Background

Previous studies [4][5] have investigated the formation of sharp edged crater lips induced by the impact of MMOD particles on International Space Station (ISS) handrails as a possible source of glove damage. In [4] hypervelocity impact tests were performed on metal plates representative of materials and thicknesses used for ISS handrails. Crater lip profiles were evaluated for impacts using 1 mm diameter spherical projectiles at ~7 km/s with varying angles of obliquity (0°-75°). For non-penetrating impacts, the authors recorded crater lip heights of 0.1-1.4 mm. For penetrating impacts, front and rear-side crater lip heights of up to 1.4 mm and 3.1 mm respectively were measured. Sharp-edges were observed on the crater lips in both non-penetrating and penetrating impacts, an example of which is shown in Figure 5.

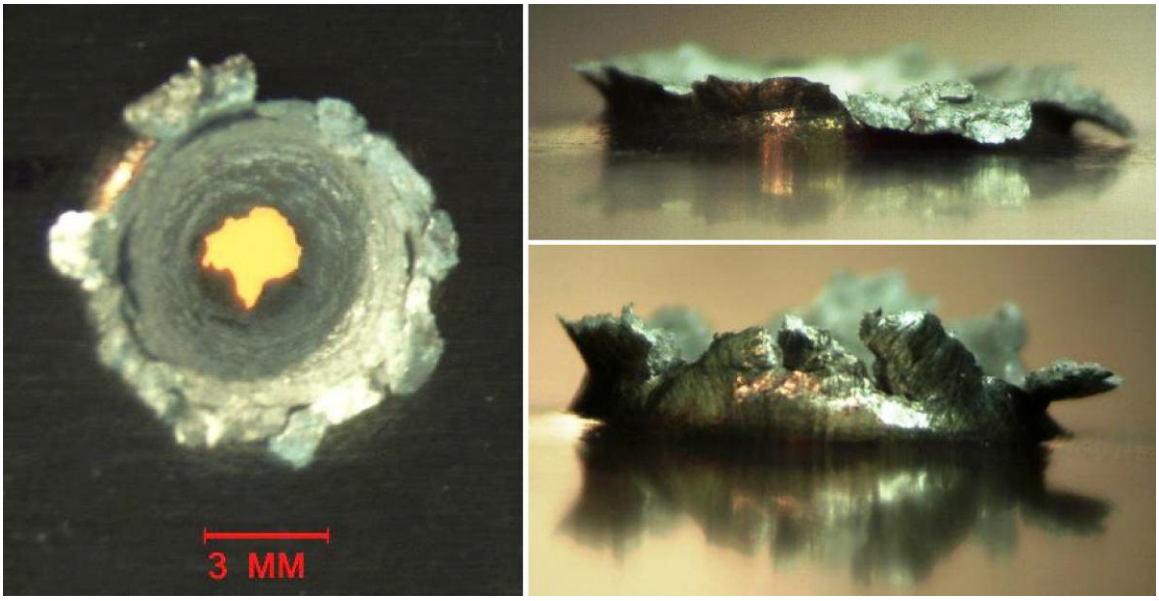

Figure 5: Crater formation in a 0.48 cm thick Al6061-T6 plate impacted at normal incidence (0°) by a 0.15 cm diameter Al2017-T4 sphere at 6.86 km/s. Left: front view; Right: side view of entry (upper) and exit (lower) crater lips.

The investigations into crater lip formation on ISS handrails was continued in [5], considering crater formation on actual flight hardware instead of the handrail-representative plates used in [4]. An example of a handrail target used in the study is shown in Figure 6.

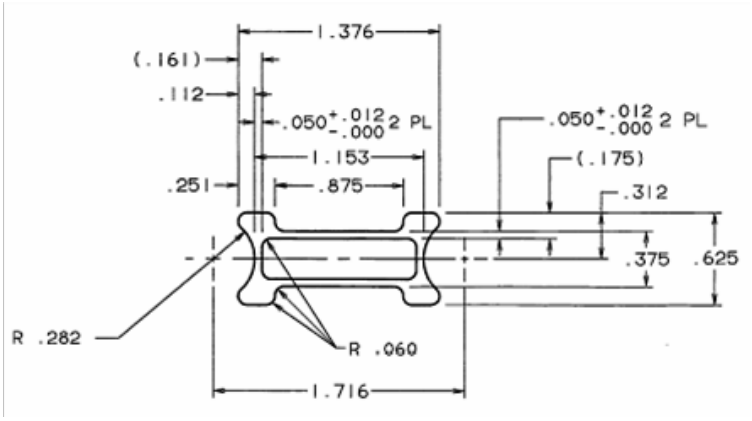

Figure 6: ISS tube handrail (P/N SDD33107728-073) subject to HVI testing in [5].

The handrails were subject to normal and oblique (45°) impact by aluminum spheres 1.0 - 2.0 mm in diameter at ~6.8 km/s. Different impact locations on the handrail structure were considered in order to replicate a wide range of possible in-flight scenarios. For non-penetrating impacts, the authors recorded crater lip heights of 0.9-2.0 mm. For penetrating impacts, front and rear-side crater lip heights of up to 2.0 mm and 4.6 mm respectively were measured. Sharp-edges were observed on the crater lips in both non-penetrating and penetrating impacts, an example of which is shown in Figure 7.

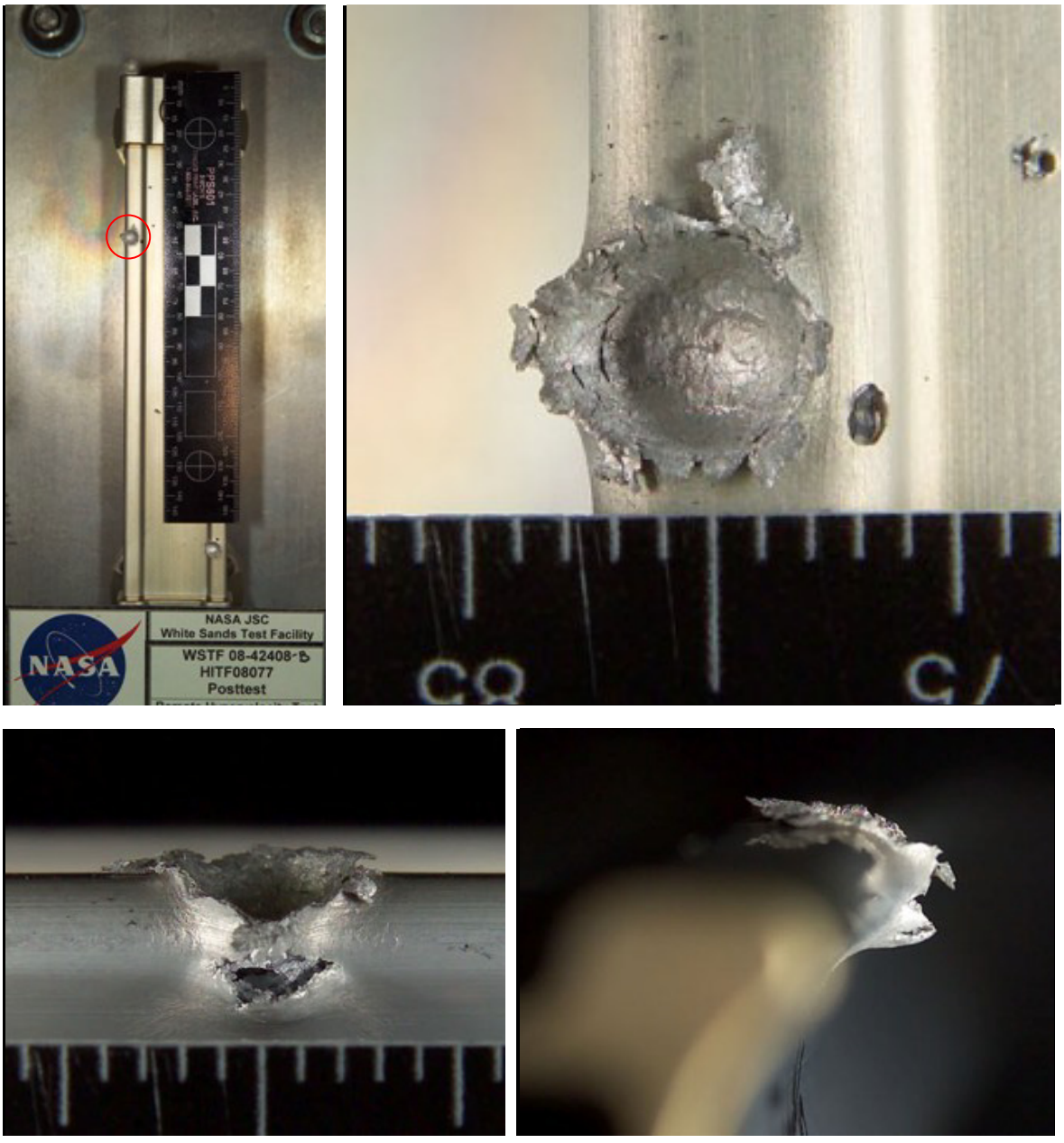

Figure 7: Crater formation on an ISS handrail resulting from oblique (45°) impact of a 1.0 mm diameter Al2017-T4 sphere at 6.94 km/s. Maximum crater lip height measured as 1.7 mm on side of handrail.

Test Articles and Target Setup

The baseline target configuration used in this study was 4.826 mm (0.19") thick Al6061-T6. This target is representative of the materials and thicknesses used in ISS handrails and hardware handled by EVA crew.

Handrail Overwraps

Four handrail overwrap configurations were considered in the test program. In all cases the overwrap is held in place directly on the surface of the baseline Al6061-T6 plate via a target frame. In Table 1 an overview of the overwrap configurations and materials is provided. For each configuration an uncompressed and compressed thickness measurement is provided. The flexible overwrap is intended to limit contact between EVA crew gloves and MMOD impact sites representing cut hazards. Therefore the performance of the overwrap must be evaluated in terms of cut hazard profile height and overwrap thickness when compressed by EVA crew gripping the handrail. Compressed thickness was measured by compressing the overwrap configuration with a 30 kg steel block. Although significantly less than the handrail design requirements for crewmember induced loads (200 lbs over a 3 inch length [6]), the variance in measured residual thickness is expected to be minimal.

Table 1: Handrail overwrap configuration details.

Type	Description	Uncompressed thickness (mm)	Compressed thickness (mm)	Areal density (g/cm^2)
FRSI	Silicon rubber coated felt-reusable surface insulation	3.89	2.15	0.182
OCF+BC	Non-reticulated open cell polyether polyurethane foam with aluminized beta-cloth cover	12.72	1.95	0.131
DROCF+BC	Double layer reticulated open cell polyether polyurethane foam with aluminized beta-cloth separator and cover	12.74	1.98	0.100
Beta-cloth	16 layers of aluminized beta-cloth with Dacron netting spacers	3.175	2.70	0.463

FRSI Overwrap

Felt-Reusable Surface Insulation (FRSI) is a silicone rubber coated Nomex felt used as part of the Space Shuttle thermal protection system (TPS) on areas which do not exceed 400°C (750 F) during ascent. These include: fuselage top and sides, payload bay doors, tops of the winds, and the Orbiter Maneuvering System (OMS) pods near the tail (see Figure 8).

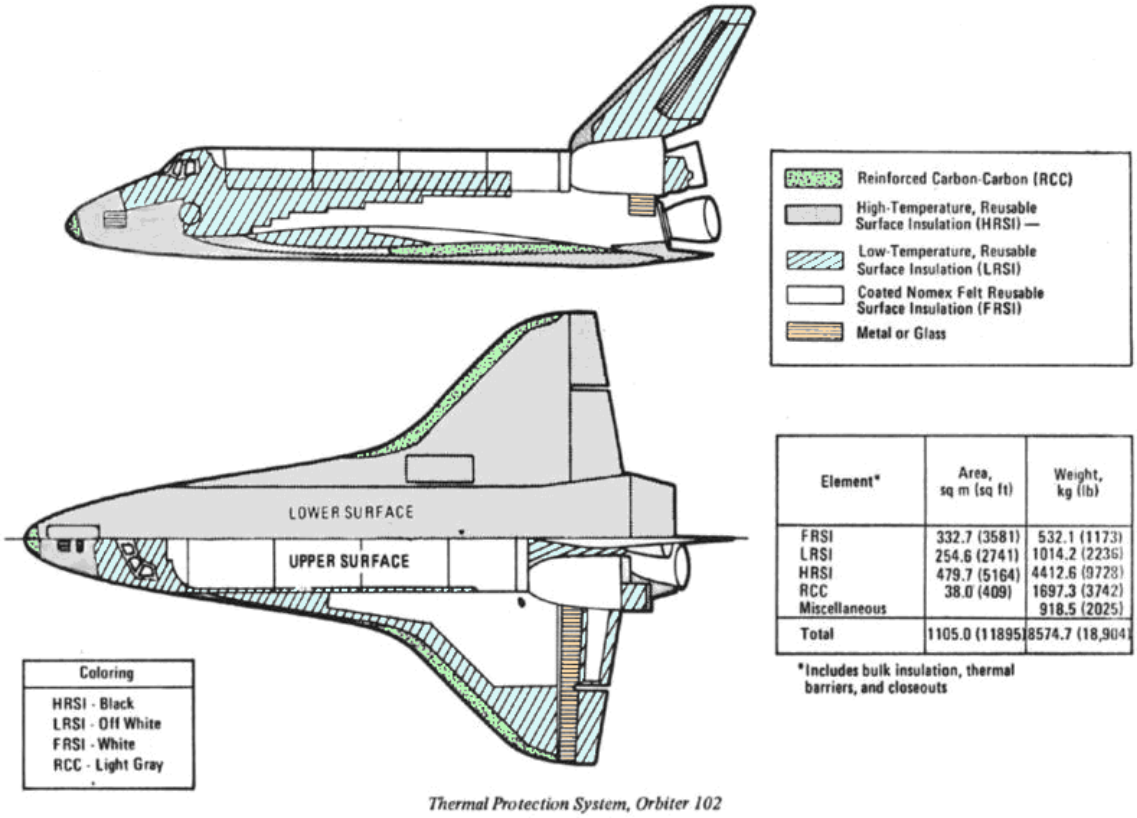

Figure 8: Thermal Protection System constituent materials (Space Shuttle Columbia).

The silicon rubber coating of the FRSI has a thickness of 127-203 μm (5 – 8 mils). The Nomex felt contains fibers nominally 76.2 mm (3.0”) in length and 2.0 denier. The configuration used in this test program has an uncompressed thickness of 3.89 mm (0.153”) and a fully compressed thickness of 2.15 mm (0.085”). The areal density of the FRSI overwrap is 0.1823 g/cm^2 (measured). The FRSI is shown in Figure 9.

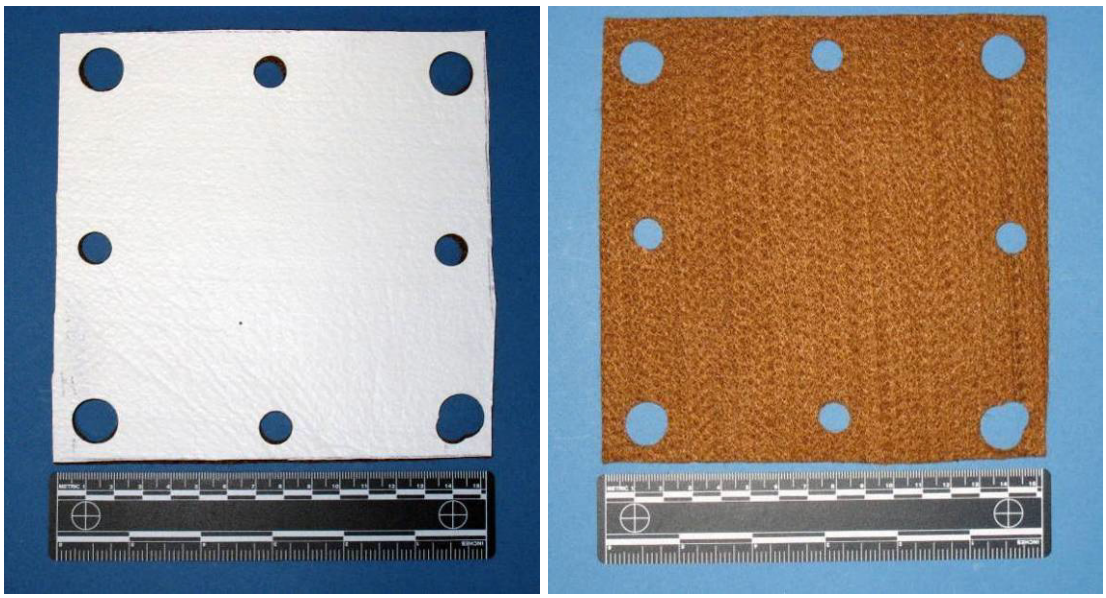

Figure 9: Felt-Reusable Surface Insulation (FRSI). Left: front view; Right: rear view.

A schematic and photo of the FRSI overwrap target set-up is given in Figure 10.

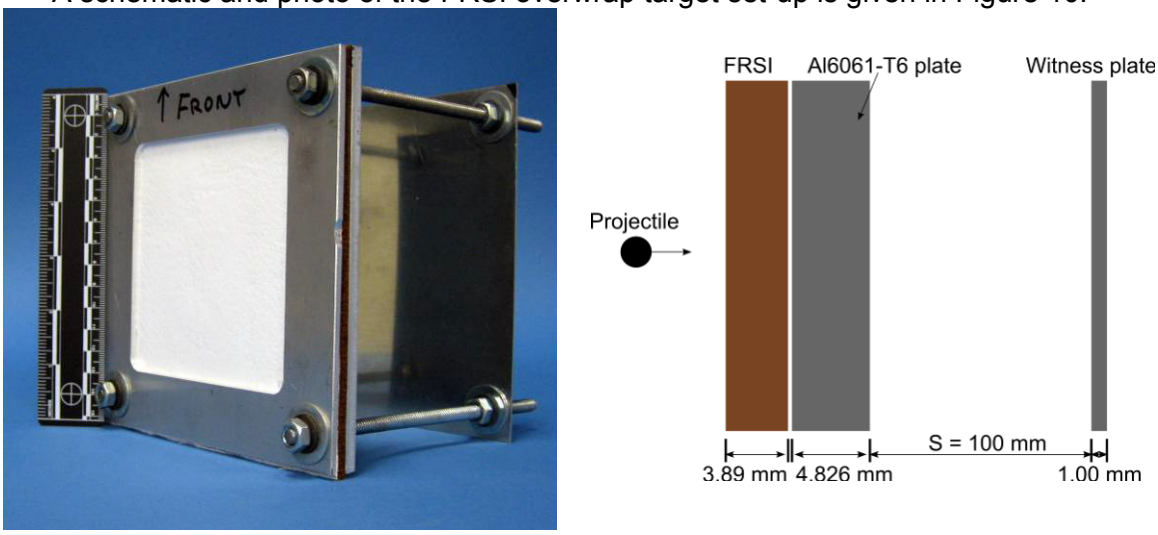

Figure 10: Photograph and schematic of the FRSI overwrap target configuration.

Open-cell polyurethane foam overwrap with beta-cloth cover (OCF+BC)

This configuration is comprised of an open-cell, non-reticulated polyether polyurethane flexible foam with an outer layer of Beta-cloth. The foam is sold under the trade name Hyfonic® from Stephenson & Lawyer, and has a nominal uncompressed thickness of 12.7 mm (0.5”), a volumetric density of 0.0293 g/cm^3, a pore density of 65 ppi, and a tensile strength of 96.53 kPa. Photographs of the foam are shown in Figure 11. A single layer of 20 micron thick aluminized Beta-cloth is placed on top of the foam, with the aluminized side facing downrange (i.e. against the foam). Beta-cloth is a non-flammable glass fiber cloth with very small diameter fibers currently used in the EMU as well as various multi-layer insulation (MLI) configurations. The beta cloth has an areal density of 0.0284 g/cm^2. When fully compressed, the measured thickness of the overwrap is 1.95 mm (0.077”). The total areal density is 0.131 g/cm^2 (measured).

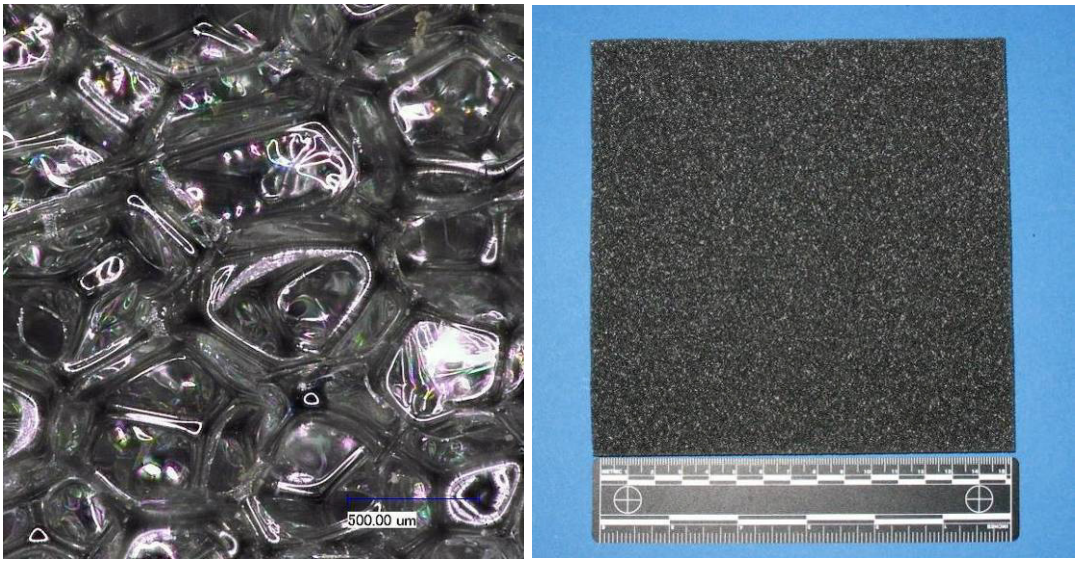

Figure 11: Open-cell non-reticulated polyurethane foam. Left: microstructure; Right: front view.

A schematic and photograph of the polyurethane foam/beta-cloth overwrap target set-up is given in Figure 12.

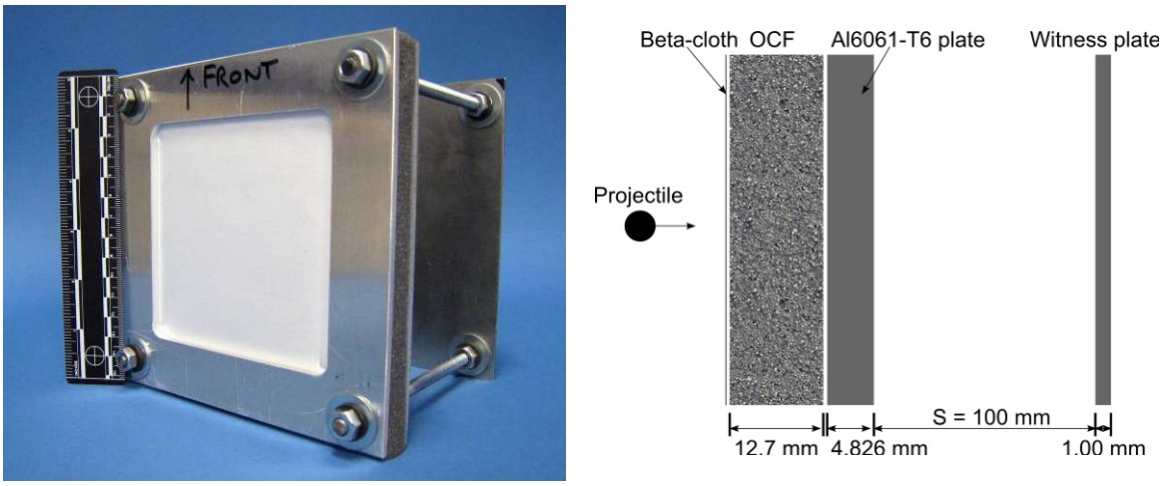

Figure 12: Photograph and schematic of the non-reticulated polyurethane open-cell foam/beta-cloth (OCF+BC) overwrap target configuration.

Double-layer open-cell polyurethane foam overwrap with beta-cloth cover (DROCF+BC)

This overwrap configuration comprises two layers of open-cell reticulated polyether polyurethane foam, alternating with two layers of aluminized beta-cloth. The foam has an uncompressed thickness of 6.35 mm (0.25”) per layer, a volumetric density of 0.034 g/cm^3, and a pore density of 20 PPI (measured). Reticulation is a process that removes the membrane between foam cells, leaving a skeletal structure behind with significantly lower density than a traditional open-cell foam (up to 97% void volume). The ligaments of the foam skeletal structure have a diameter of ~25 microns. Layers of 20 micron thick aluminized beta-cloth are placed between the foam layers, and on the upper surface of the configuration, with the aluminized side facing downrange in both instances. The beta cloth has an areal density of 0.0284 g/cm^2. When fully compressed, the measured thickness of the overwrap is 1.98 mm (0.078”). The total areal density of the configuration is 0.100 g/cm^2.

A schematic and photograph of the double-layer polyurethane foam/beta-cloth overwrap target set-up is given in Figure 14.

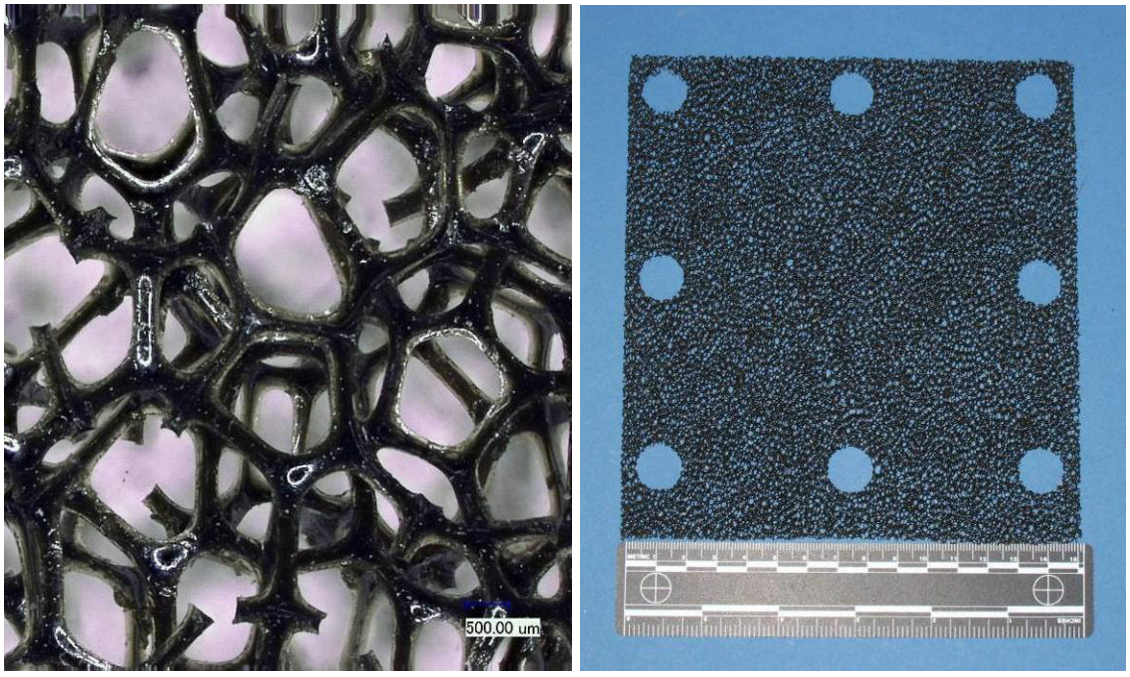

Figure 13: Open cell reticulated polyether polyurethane foam. Left: foam microstructure; Right: front view.

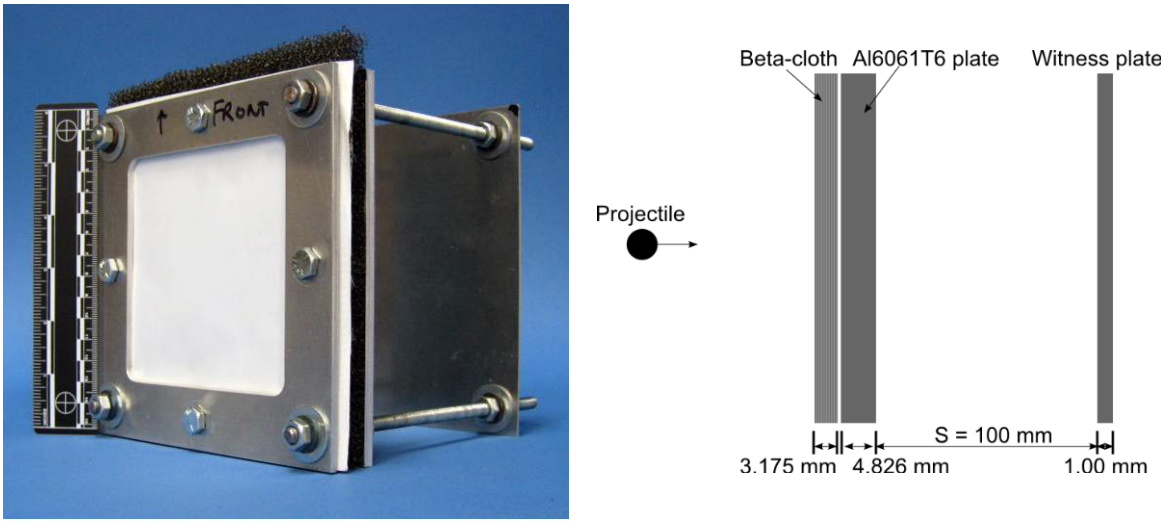

Figure 14: Photograph and schematic of the double layer reticulated polyurethane open-cell foam/beta-cloth (DROCF+BC) overwrap target configuration.

Beta-cloth overwrap (Beta-cloth)

The beta-cloth overwrap is made of 16 layers of 20 micron thick aluminized beta-cloth, separated by Dacron netting spacers (commonly used in MLI). The total uncompressed thickness of the configuration is 3.175 mm (1/8”). When fully compressed the thickness is reduced to 2.70 mm (0.106”). The overwrap is held in place via a target frame, while the fabric is stretched to minimize billowing. For all layers, the aluminized side of the beta-cloth is facing downrange. The total areal density of the Beta-cloth overwrap is 0.463 g/cm^2.

A schematic and photograph of the Beta-cloth overwrap target set-up is given in Figure 15.

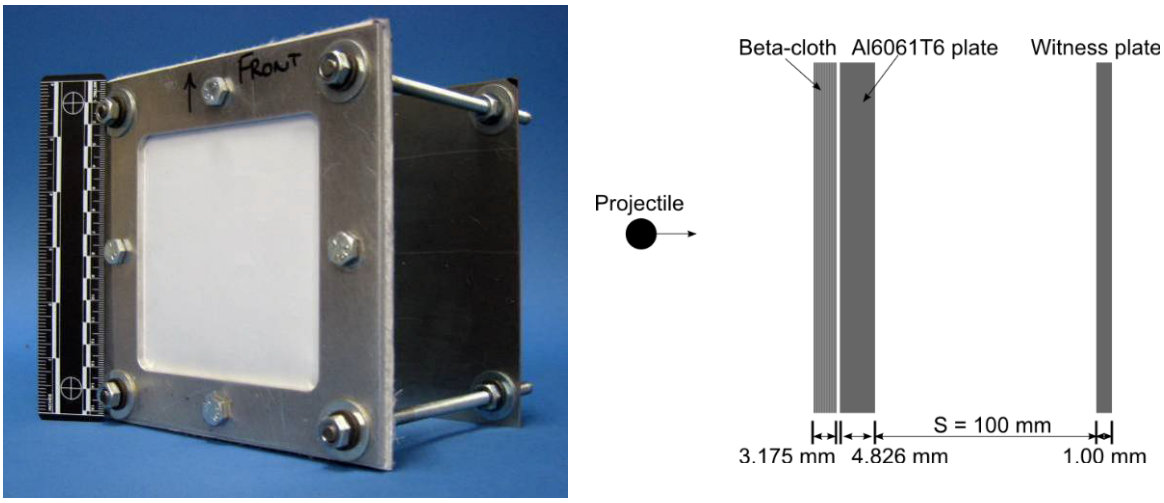

Figure 15: Photograph and schematic of the beta-cloth overwrap target configuration.

Alternate Handrail Materials

For flight hardware yet to be constructed, alternate materials for ISS handrails that do not generate hazardous crater edges when impacted by MMOD particles are of interest. During hypervelocity impact of MMOD particles, an evacuation flow develops behind the shock wave during projectile penetration (i.e. “splash-back”). For ductile materials, this evacuation flow acts to form an uprange crater lip once the material is sufficiently cooled. For brittle materials, limited plastic flow minimizes the formation of protruding crater lips.

Four alternate handrail materials were evaluated in the test program. Three fiber reinforced composites, and one fiber/metal laminate were selected based on their equivalent or superior specific tensile modulus and strength properties. The tensile strain to failure of the four materials was in all cases, significantly less than that of the baseline handrail material. An overview of the alternate handrail materials is provided in Table 2. A comparison of key mechanical properties is made in Table 3.

Table 2: Alternate handrail materials subject to testing.

Type	Description	Thickness (mm)	Areal density (g/cm^2)
MMC	Continuous Nextel 610 fiber reinforced pure aluminum (V_f = 40%)	3.3 mm	1.089
CFRP	Quasi-isotropic IM7/954-2A carbon fiber reinforced plastic	7.03 mm	1.09
Fiberglass	Woven glass fabric/halogen-free epoxy type NP500CR	4.826 mm	0.869
FML	Fiber metal laminate with alternating layers of Al2024-T3 and S-2/FM94 glass/epoxy composite	3.74 mm	0.811

Table 3: Mechanical properties of common ISS handrail materials and alternative candidates.

Material	Bulk density (g/cm^2)	Tensile modulus (GPa)	Tensile strength (MPa)	Tensile strain to failure (%)
Al 6061-T6	2.70	68.9	310	12-17
SS 15-5PH	7.80	200	1145	17
Nextel 610/Pure Al (typical properties)	3.30	207	1450	0.7
IM7/954-2A CFRP (micromechanics)	1.564	167	3105	2.0*
NP500CR fiberglass	1.80	27.5*	310	5.7*
GLARE	2.17	50*	300*	4.5*

* Assumed properties

Metal Matrix Composite (MMC)

The metal matrix composite selected for impact testing was manufactured by Touchstone Research Laboratory. The composite consisted of four 0.66 mm (0.026") nominally thick u.d. plies of Nextel 610 ceramic fiber with a pure aluminum metal matrix (40% fiber content by volume). The stacking sequence of the u.d. plies was given as 0°/90°/90°/0°. Photos of the material and target assembly are shown in Figure 16 and Figure 17. The target sample measures 2.54×2.54cm (1"×1") and was mounted in a recessed frame with a 1.9x1.9cm (0.75"×0.75") opening during impact testing.

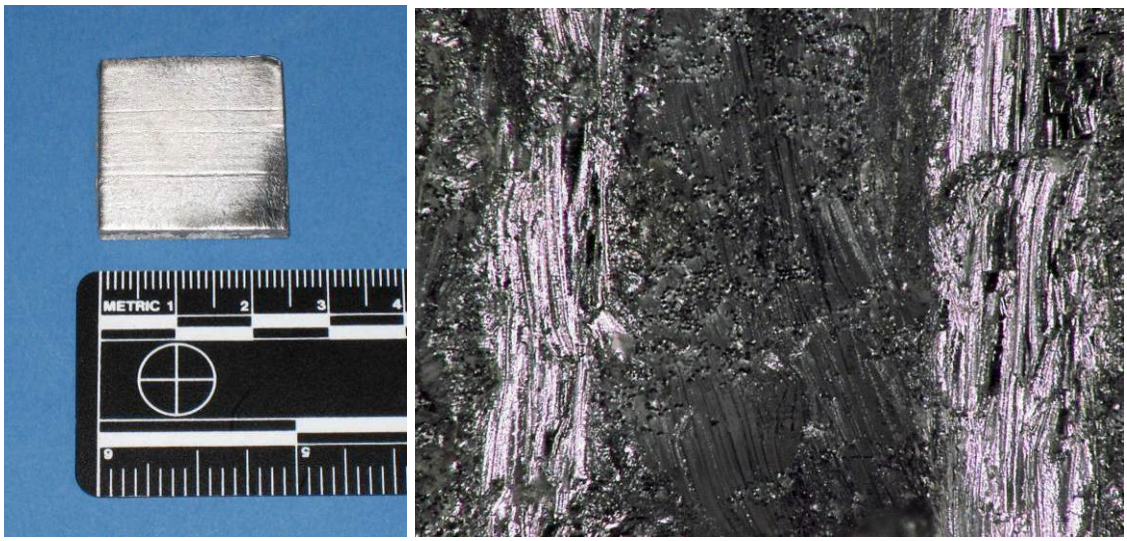

Figure 16: Nextel/Al metal metrix composite. Left: test sample; Right: magnified view showing individual layer orientations within the composite laminate.

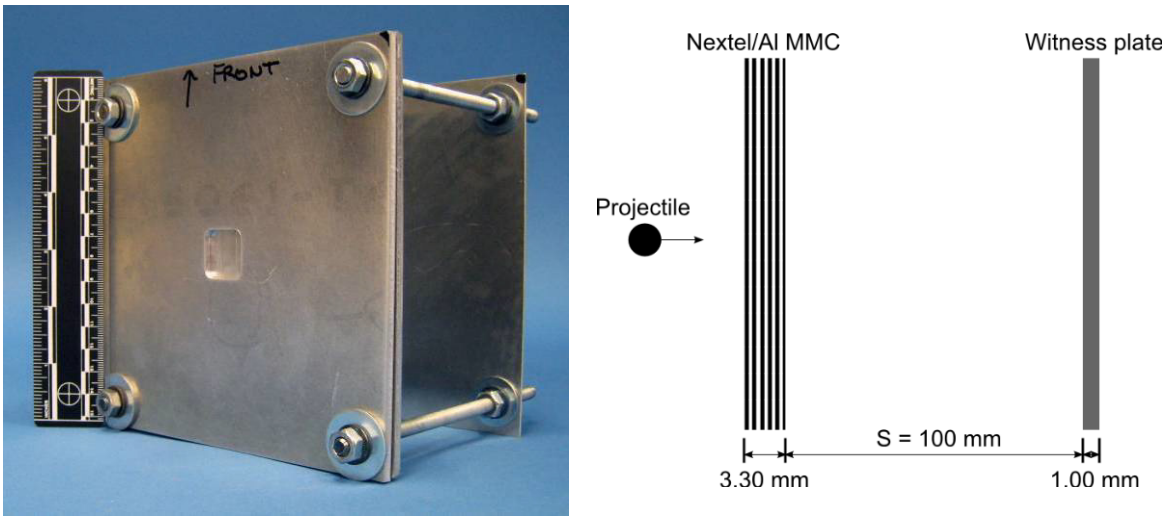

Figure 17: Photograph and schematic of the Nextel/Al MMC target configuration.

Carbon Fiber Reinforced Plastic (CFRP)

The CFRP selected for testing was manufactured for use as an external skin onboard NASA's X-38 Crew Return Vehicle (CRV). The panel is 7.03 mm thick, consisting of 48 u.d. plies of IM7 type fiber with 954-2A cyanate ester resin (60% fiber content by volume), a plain weave IM7/954-2A fabric cover on one side, and a film of Araldite AF191 adhesive imbedded with a fine copper mesh on the other. The stacking sequence of the u.d. plies is $[0°/+45°/90°/-45°/0°/+45°/90°/-45°/0°/+45°/90°/-45°/0°/+45°/90°/-45°/0°/+45°/90°/-45°/0°/+45°/90°/-45°]_s$. The plain weave pattern of the upper layer is shown in Figure 18 along with a microscopic image clearly showing ply orientation differentiation.

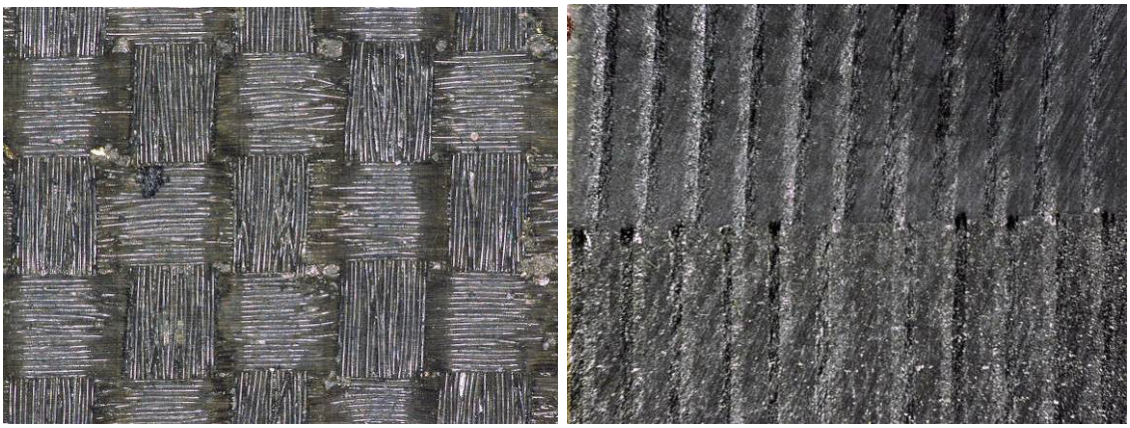

Figure 18: Visual inspection of the CFRP target material. Left: outer fabric layer plain weave (x200 magnification); Right: varying orientation of the u.d. layers (x30 magnification).

The CFRP target was impacted on the side of the woven fabric layer in order to mitigate the influence of the copper reinforced adhesive layer. The test sample had lateral dimensions of 152.4×152.4 mm and was mounted in a target frame. A 1 mm thick Al6061-T6 witness plate was spaced 100 mm from the target rear side using threaded rods. A schematic and photograph of the target configuration are shown in Figure 19.

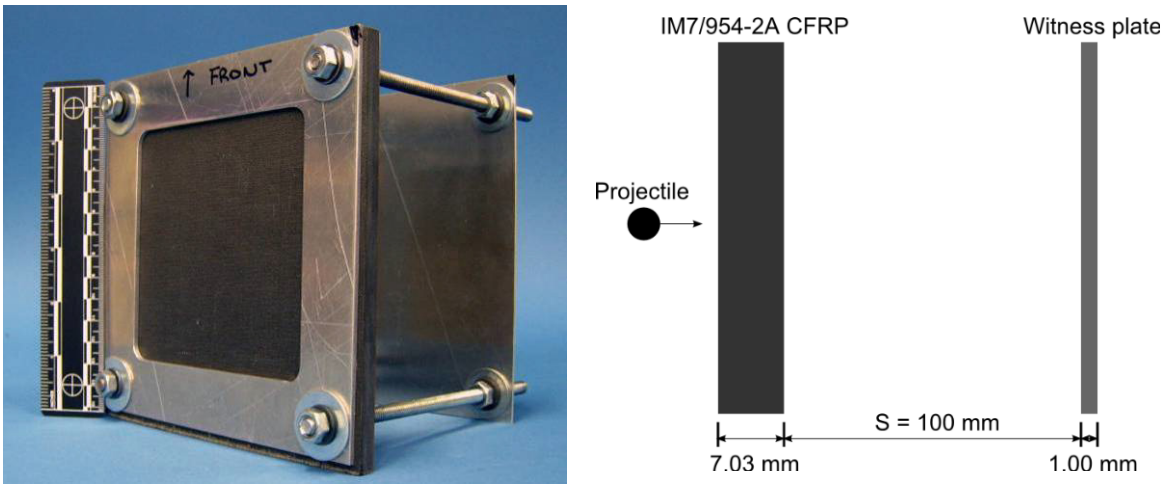

Figure 19: Photograph and schematic of the IM7/954-2A CFRP target configuration.

Fiberglass

A 4.83 mm (0.19”) thick woven glass fabric/halogen-free epoxy resin system produced by Norplex-Micarta with the trade name NP500CR was selected as another alternative material for ISS handrails. NP500CR is manufactured to the National Institute of Standards and Technology (NIST) G-10CR process specifications for deep space and cryogenic applications and is currently in use onboard NASA’s STEREO satellite. A photograph and schematic of the fiberglass target are shown in Figure 20.

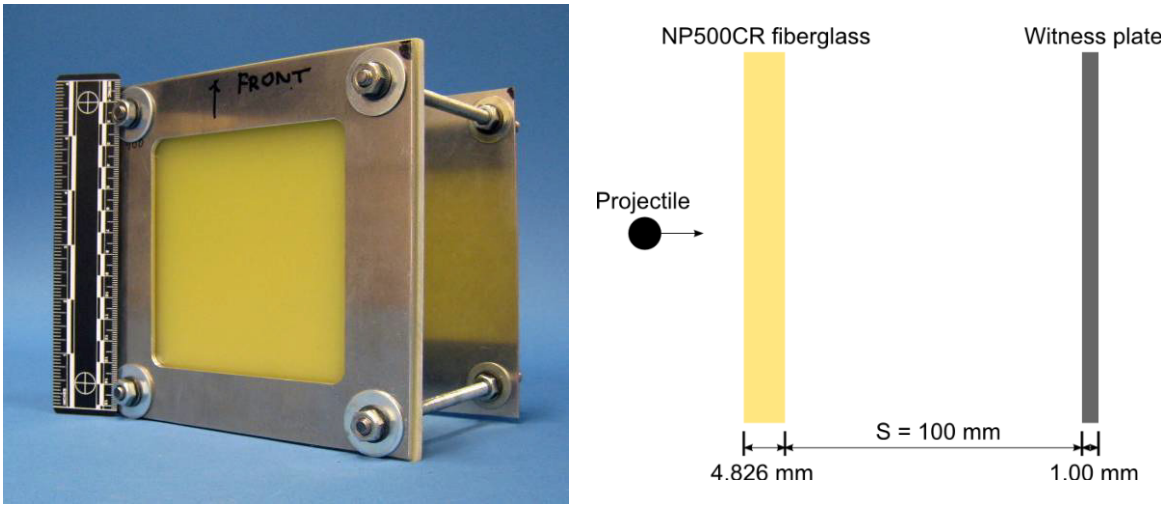

Figure 20: Photograph and schematic of the NP500CR fiberglass target configuration.

Fiber Metal Laminate (FML)

Glare© is a glass fiber reinforced fiber metal laminate consisting of alternating layers of Al2024-T3 and uni-directional S-2/FM94 glass fiber/epoxy composite. Glare is currently used in the upper fuselage of the Airbus A380, and explosive containing devices (e.g. hardened aircraft cargo carrier). The fiber composite reinforcement increases the tensile and fatigue strength of the baseline aluminum, and have shown

promising performance in explosive testing as a result of high strain-rate strengthening of the glass fibers [7]. A 3.74 mm (1.47”) thick Glare sample was selected for testing with a stacking sequence of [Al/0°/90°/90°/0°/0°/90°/Al/90°/0°/0°90°/90°/0°/Al/0°/90°/90°/0°/0°/90°/Al], referred to as Glare 7, 4/3 (i.e. 7 total layers, 4/3 ratio of aluminum to glass/epoxy layers). Photos of the material and target assembly are shown in Figure 21 and Figure 22.

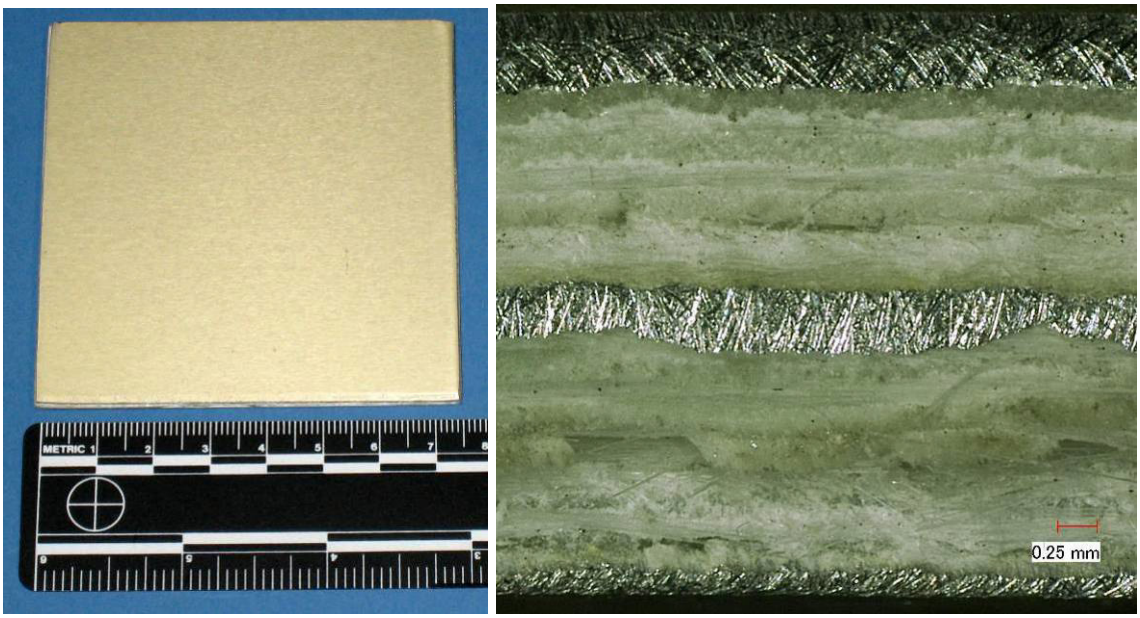

Figure 21: Glare fiber metal laminate. Left: top view; Right: magnified view showing individual aluminum and glass composite layers.

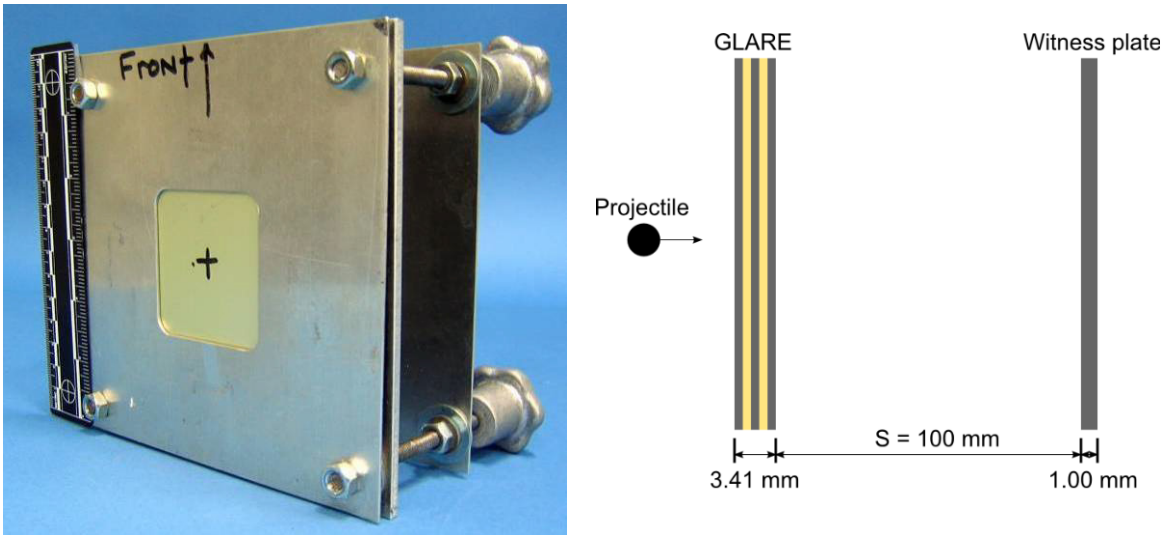

Figure 22: Photograph and schematic of the Glare fiber metal laminate target configuration.

Test Results

Eight impact tests were performed on the handrail overwrap targets, two shots on each configuration. An overview of test impact conditions and key damage measurements is provided in Table 4. Descriptions of overwrap and handrail damage measurements are shown in Figure 23 and Figure 24. Four hypervelocity impact tests were performed on alternate materials for ISS handrails, one test on each of the four material candidates. An overview of test impact conditions and key damage measurements is provided in Table 5.

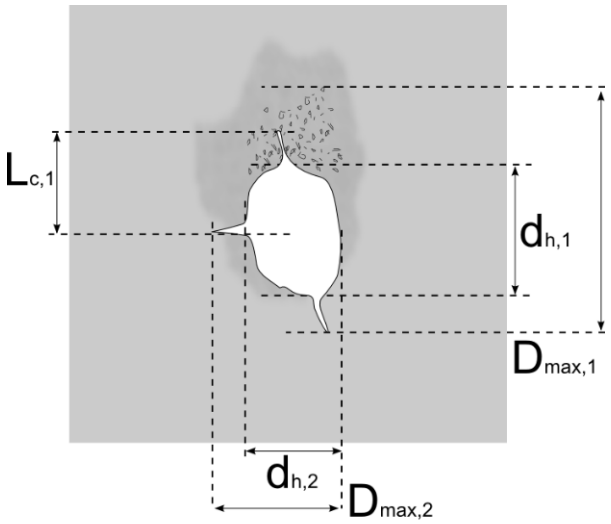

Figure 23: Definition of handrail overwrap damage measurements.

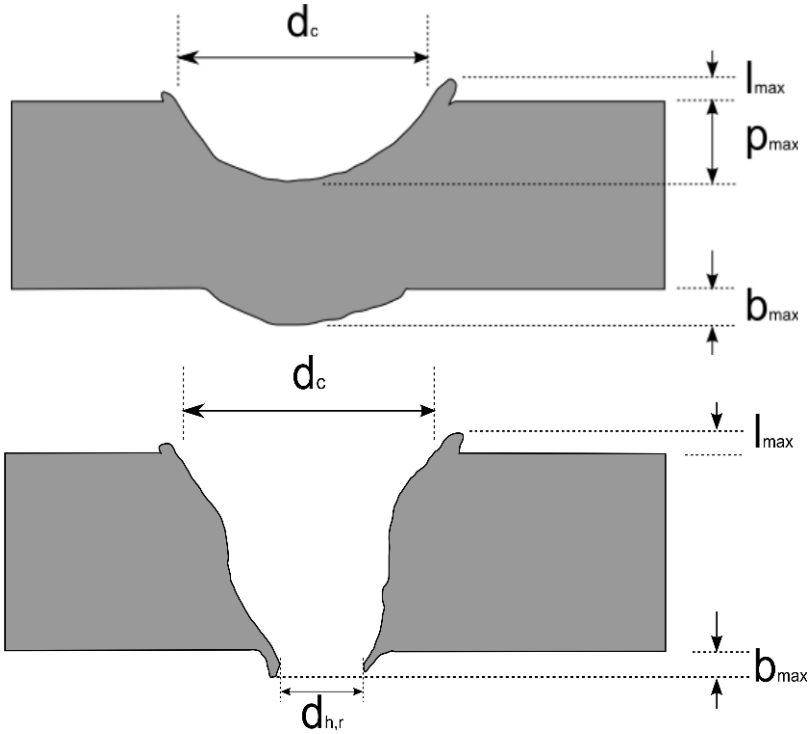

Figure 24: Definition of handrail damages. Top: cratered handrail. Bottom: perforated handrail.

Table 4: Handrail overwrap test results and damage measurements.

	Test No.	Target	Projectile			Impact conditions		Damage measurements					
								Overwrap			Target		
			Material (-)	Diameter (mm)	Mass (mg)	Velocity (km/s)	Angle (deg)	$d_{h,f}$ (mm)	$D_{max,f}$ (mm)	$d_{h,r}$ (mm)	d_c (mm)	l_{max} (mm)	p_{max} (mm)
1	HITF08282	FRSI	Al2017-T4	1.0	1.46	6.55	0	1.7×1.7	5.1×4.5	3.0×3.0	3.4×3.4	0.3	1.2
2	HITF08242	FRSI	Al2017-T4	1.5	4.60	6.95	45	6.4×18.3	16.8×20.3	4.2×8.9	4.7×6.5	0.7	1.2
3	HITF08283	OCF+BC	Al2017-T4	1.0	1.47	6.98	0	1.5×1.3	1.6×1.3	8.5×7.2	1.1×1.3	0.1	0.9
4	HITF08243	OCF+BC	Al2017-T4	1.5	4.86	6.85	45	5.7×9.7	5.8×9.8	9.9×12.1	3.1×3.1	0.3	1.5
5	HITF08284	DROCF+BC	Al2017-T4	1.0	1.43	6.99	0	1.3×1.3	1.4×1.4	4.4×4.9	1.0×1.0	0.1	0.1
6	HITF08244	DROCF+BC	Al2017-T4	1.5	4.80	7.03	45	2.0×3.3	2.0×3.4	17.4×22.5	2.3×2.5	0.8	1.4
7	HITF08250	Beta-cloth	Al2017-T4	1.0	1.47	6.86	0	2.2×2.2	3.7×3.3	4.3×5.4	<0.1	<0.1	0.0
8	HITF08245	Beta-cloth	Al2017-T4	1.5	4.82	6.94	45	2.2×5.3	8.8×17.7	4.1×4.6	<0.1	<0.1	0.0

Table 5: Alternate handrail material test results and damage measurements.

	Test No.	Target	Projectile			Impact conditions		Damage measurements					
			Material (-)	Diameter (mm)	Mass (mg)	Velocity (km/s)	Angle (deg)	$d_{c,f}$ (mm)	$D_{max,f}$ (mm)	$p_{max,f}$ (mm)	$l_{max,f}$ (mm)	$d_{h,r}$ (mm)	b_{max} (mm)
1	HITF08247	MMC	Al 2017-T4	1.0	1.42	6.87	0	4.3×3.0	5.6×5.4	n/a	1.00	11.3 x 7.7	2.45
2	HITF08248	CFRP	Al 2017-T4	1.0	1.41	6.91	0	2.1×2.1	5.2×79.6	2.7	0.0	n/a	n/a
3	HITF08249	Fiberglass	Al 2017-T4	1.0	1.42	6.86	0	2.6×2.6	7.6×7.6	0.6	0.8	n/a	0.3
4	HITF08330	FML	Al 2017-T4	1.0	1.45	6.99	0	8.3×9.7	10.8×12.5	0.3	3.5	n/a	1.69

Analysis and Discussion

Normal impact of a 1.0 mm Al2017-T4 sphere at ~6.77±0.22 km/s on an unshielded 4.826 mm thick Al6061-T6 plate in [4] resulted in a 4.2 mm diameter crater that had a maximum depth of 2.2 mm and a lip that protruded a maximum of 1.0 mm above the target surface. All four overwrap configurations were able to significantly reduce the diameter, depth and protruding lip height of the simulated handrail impact crater. For oblique (45°) impact of a 1.5 mm Al2017-T4 sphere at 6.94±0.09 km/s on an unshielded 4.826 mm thick Al6061-T6 plate in [4], a 2.9 mm deep crater was formed with a diameter of 6.9 mm (maximum) and a raised lip height of

0.8 mm. All four overwrap configurations were capable of reducing the crater depth and diameter, however only the beta-cloth and OCF+BC overwraps were effective at reducing the crater lip height.A comparison between the impact generated crater in the unshielded handrail (from [4]) and the handrails protected by the overwraps is given in Figure 25 (for normal tests) and Figure 26 (for oblique tests). In Figure 25 it can be seen that the impact crater in the unshielded handrail is clearly defined with a well-formed lip protruding above the plate surface. Of the overwrap configurations, only the FRSI target shows a cleanly formed crater with a discernable lip, however the diameter of the crater and height of the protruding lip are clearly smaller than that of the baseline target. The target plate wrapped by the OCF+BC configuration shows a small crater and a number of deposits and dents in the target surface, however there is very little protrusion above the target plane. The target plates covered with the DROCF+BC and Beta-cloth configurations show no discernable crater formation, only some discoloration and shallow denting of the target surface. For the oblique tests a clearly formed crater and protruding crater lip is observed on the unshielded target. Cratering of the target plate is apparent on the FRSI target as well as that of the OCF+BC and DROCF+BC. Only the Beta-cloth configuration appears to have prevented formation of any impact crater. On the FRSI target the crater is cleanly formed and has a clearly observable lip protruding from the target surface. For the OCF+BC configuration, multiple overlapping craters can be observed, suggesting fragmentation of the projectile during impact with the overwrap. Although the craters are cleanly formed, there is minimal protrusion of material above the target surface. A similar damage profile is seen on the DROCF+BC target, which shows a single cleanly formed crater (albeit with diameter significantly smaller than that of the unshielded target) with minimal protrusion of the crater lip above the target surface. The Beta-cloth configuration shows minimal damage to the target plate.

Of the four configurations tested, the beta-cloth overwrap proved the most effective at limiting damage to the underlying metallic handrail. Given the comparatively large areal density of the beta-cloth overwrap (0.463 g/cm^2), this is to be expected. The only configuration to show a significant amount of damage to the outer surface was the FRSI overwrap in the oblique impact tests. It is important to note, however, that this damage was predominantly a removal of the silicon rubber coating and did not significantly reduce the thickness of the underlying Nomex felt. Considering the compressed thickness of the four overwrap configurations is larger than the measured crater lip height in all 8 impact experiments, all four overwrap configurations must be considered successful in preventing contact between EVA crewmember gloves and MMOD cut hazards (for the specific impact conditions and handrail configuration tested).

In Table 5 two of the four alternate materials tested were shown to reduce the lip height of MMOD craters compared to a baseline Al6061-T6 target when impacted by a 1.0 mm diameter Al2017-T4 sphere at normal incidence with a velocity of 6.91±0.08 km/s. There was no measurable crater lip on CFRP laminate, however there was a degree of surface spallation about the impact site, including groups of single ply thick material that protruded above the target surface. Surface spallation is limited by the outer plain weave fabric layer (compared with a u.d. outer layer), however it is still considered that the surface spallation may be hazardous to EMU gloves (potentially more so than the sharp crater lips on metallic handrails). As such, this particular CFRP laminate is considered unsuitable as a potential material for ISS handrails. By increasing the number of fabric layers on the outer surfaces of the laminate, the degree of surface spallation can be reduced, which should be considered in any further investigations. The other material to decrease the height of the cut hazard was the NP500CR fiberglass.

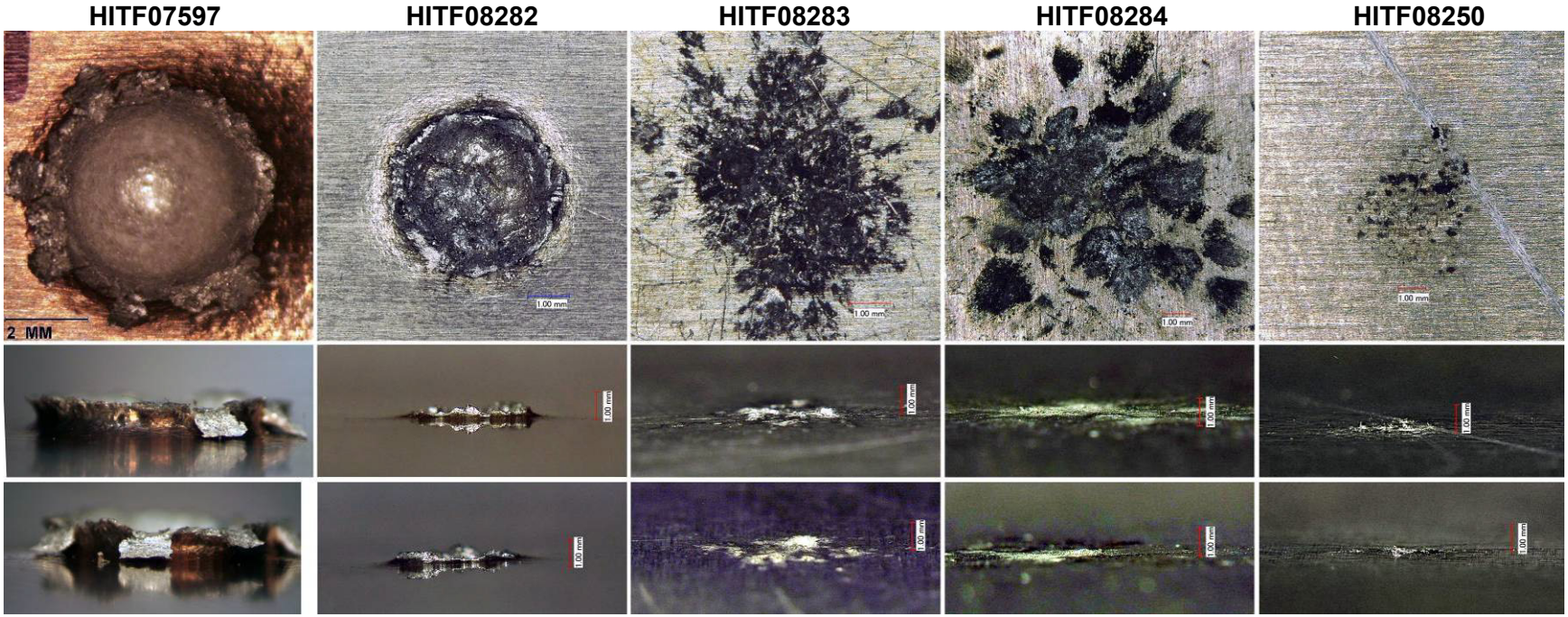

Figure 25: Comparison of impact crater profile in an unshielded Al 6061-T6 plate (representative of an ISS handrail) and overwrap shielded plates impacted by a 1.0 mm diameter Al 2017-T4 sphere at 6.77 ± 0.22 km/s with normal incidence (0°).

For this material, fractured and delaminated fibers protruded above the target surface. Unlike the CFRP laminate however, these protrusions were not rigid, nor did they extend beyond the local impact site (see Figure 27). In this case the epoxy material has been completely removed from the protruding fibers, and it is considered that the puncture hazard of the fibers is minimal. The Glare fiber metal laminate provided the largest crater lip height, 3.3 times that of the original Al6061-T6 material. As shown in Figure 27, the outer aluminum layer of the FML peeled back from the glass/epoxy composite layer during impact, resulting in a large crater diameter with very sharp petalled edges. By modifying the laminate layup such that there are a number of glass/epoxy layers on the outer surface, it is expected that the height of any damage features would be reduced. The Nextel 610/pure Al metal matrix composite provided similar performance (in terms of protruding crater lip height) to that of the baseline Al6061-T6 handrail. The Nextel fiber reinforcements act to increase the stiffness of the pure aluminum and reduce its ductility. A more brittle material would be expected to form smaller protruding crater lips given the reduced plastic flow sustained in the material.

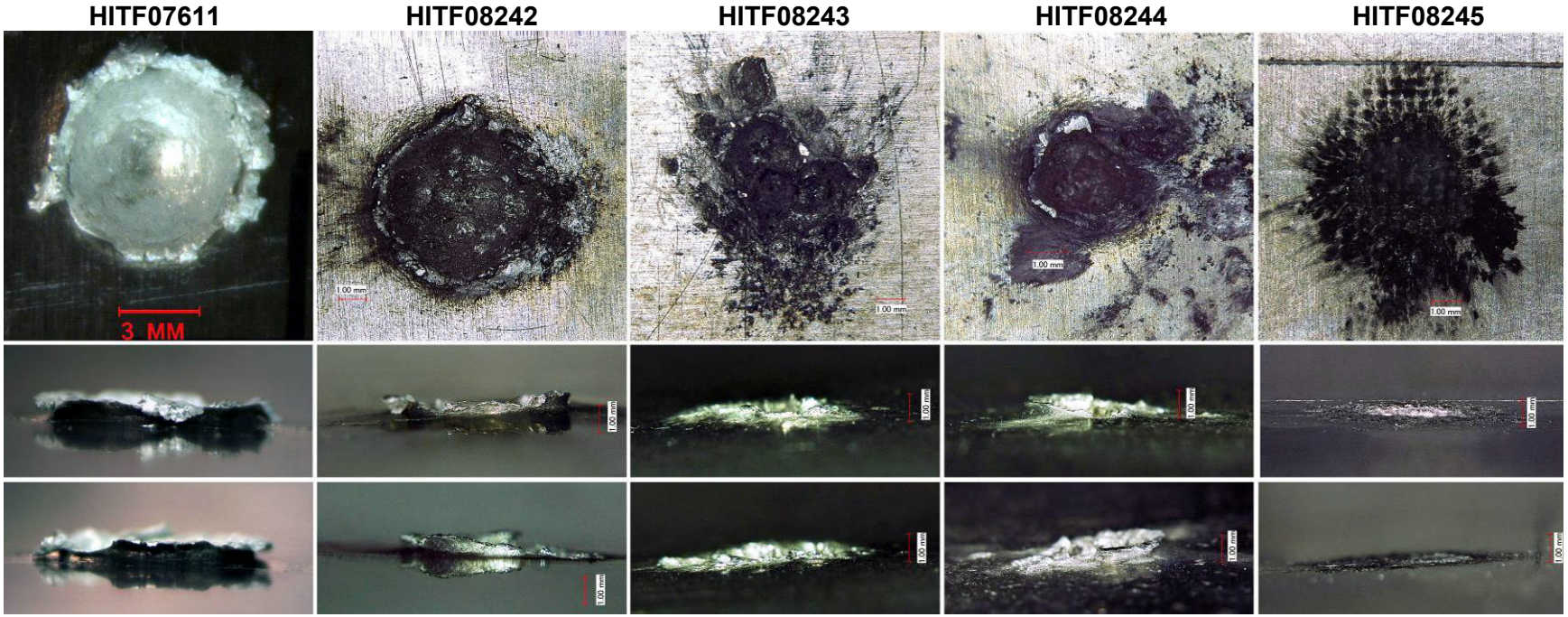

Figure 26: Comparison of impact crater profile in an unshielded Al 6061-T6 plate (representative of an ISS handrail) and overwrap shielded plates impacted by a 1.5 mm diameter Al 2017-T4 sphere at 6.94 ± 0.09 km/s with oblique incidence (45°).

In Figure 27, it can be seen that the outer layer of the MMC laminate fractured about the impact site, resulting in almost no protrusion above the target surface. Indeed, the 1.0 mm lip height was measured from the laminate 2nd layer. The MMC target is penetrated by the projectile, resulting in a rear side damage feature with a maximum height of 2.45 mm. Given that the thickness of the MMC was less than that of the baseline handrail target, this does not indicate a decreased performance. However, for penetrating impacts using a 1.5 mm and 2.0 mm projectile on the baseline Al6061-T6 target in [4], a maximum exit hole lip height of 1.9 mm was measured (normal impact). Therefore, it is considered that the performance of the Nextel 610/pure Al MMC is worse than that of the baseline aluminum alloy.

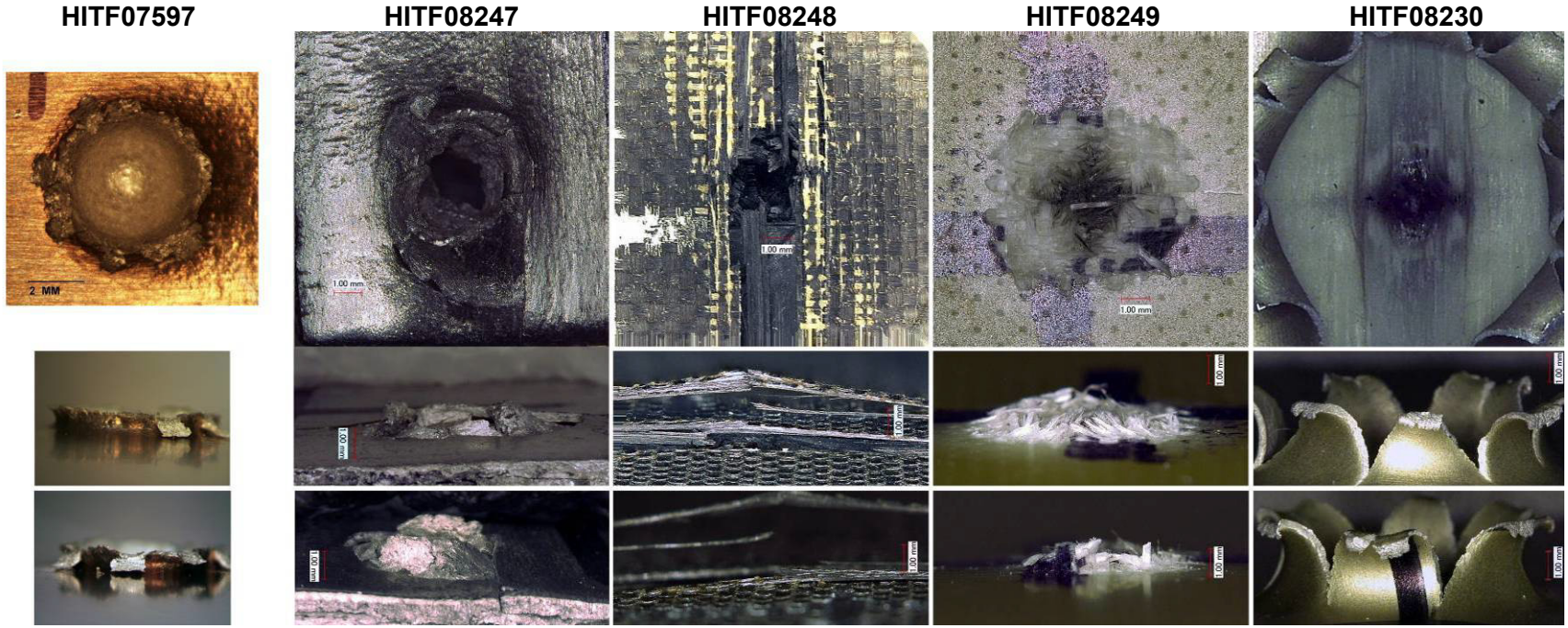

Figure 27: Comparison of impact crater profile in a simulated ISS aluminum handrail and alternate handrail materials (from left to right: Al 6061-T6, MMC, CFRP, fiberglass, FML) impacted by a 1.0 mm diameter Al 2017-T4 sphere at 6.91 ± 0.08 km/s with normal incidence (0°).

Conclusions

Exposed hardware on the ISS is subject to regular impact of micrometeoroid and orbital debris particles. When impacting on metallic surfaces, these MMOD particles generate an impact crater which can pose a cut hazard to crewmember EMU gloves during EVA. In order to reduce this hazard, two potential modifications to ISS handrails have been evaluated in this study. In the first phase of the study flexible overwrap configurations were investigated. These overwraps are suitable for retrofitting ground equipment that has yet to be flown. The purpose of the overwrap is not to protect the handrail from impact of MMOD particles, rather its purpose is to act as a spacer between hazardous impact profiles and crewmember gloves during EVA.

Towards this end, hypervelocity impact tests were performed on the overwrapped handrail-representative targets. The damage feature protrusion height was measured, and the target performance was evaluated in terms of crater lip height and the compressed thickness of the overwrap. Four configurations were tested: a felt-reusable surface insulation used on the Shuttle orbiters (FRSI), an open cell polyether polyurethane foam with an outer cover of beta-cloth (OCF+BC), a double-layer configuration with reticulated open cell polyether polyurethane foam and beta-cloth (DROCF+BC), and a multi-layer beta-cloth overwrap (16 layers) with intermediate Dacron netting spacers. All four configurations were shown to reduce the degree of damage in the handrail target, and the measured crater lip heights were in all cases less than that of the compressed overwrap thickness. There was minimal surface damage to the four overwrap configurations, suggesting that they would act successfully in preventing contact between EVA crew gloves and MMOD impact cut hazards.

In the second phase of the study alternate materials for external handrails were investigated. Four brittle materials with high specific stiffness and strength were subject to impact testing: a Nextel 610 fiber reinforced pure aluminum metal matrix composite (MMC), a quasi-isotropic carbon fiber reinforced epoxy laminate (CFRP), a woven fiberglass/epoxy composite (fiberglass), and a fiber metal laminate with alternating layers of Al6061-T6 and S-2 glass/epoxy (trade name GLARE). Of the four materials tested, only the fiberglass target was considered to form less a hazardous damage profile than the baseline Al6061-T6 target. Although the CFRP target did not generate a protruding crater lip, the spallation of carbon fibers from the outer surface of the target are considered to represent a puncture risk. The fiberglass target impact crater was smaller in diameter and lip height than the baseline material, and fragmented glass fibers about the impact site were soft and highly flexible suggesting a low puncture threat to EMU gloves. Although the GLARE FML performed significantly worse than the baseline aluminum alloy target, it is considered that by modifying the stacking sequence of the aluminum/fiberglass layers a much better performance could be gained (i.e. fiberglass outer layer).

In tandem with efforts to increase the puncture and cut resilience of Phase IV EMU gloves, the findings of this study provide a possibility to significantly reduce the cut glove hazard of MMOD impact sites on ISS handrails.

References

[1] R. Pearlman, “The worst glove damage we have seen in the history of going EVA”, collectSPACE, accessed 5/15/08, url: http://collectspace.com/ubb/Forum30/HTML/000521.html, April 13, 2007.

[2] C. Bergin, “EVA-3 terminated due to Mastracchio glove damage”, NASA spaceflight.com, accessed 5/15/08, url: http://www.nasaspaceflight.com/content/?cid=5202, August 15, 2007.

[3] C. Bergin, “STS-122 spacewalkers gain extra protection – FRR focus on EVAs”, NASA spaceflight.com, accessed 5/15/08, url: http://www.nasaspaceflight.com/content/?cid=5295, November 28, 2007.

[4] B.A. Davis, E.L. Christiansen, T. Prior, “Hypervelocity Impact (HVI) Test Plan for Crater Characterization for Cut Glove Investigation”, NASA Johnson Space Center (unpublished), 2008.

[5] B.A. Davis, E.L. Christiansen, E. Ordonez, T. Prior, “ISS Handrail Hypervelocity Impact Test Program Phase – 1”, NASA Johnson Space Center (unpublished), 2008.

[6] Anon., “Specific Design Requirements Document: Handrails/Handholds for International Space Station”, NASA Johnson Space Center, CTSD-SS-809, 1995.

[7] G. Wu, J.M. Yang, “The Mechanical Behavior of GLARE Laminates for Aircraft Structures”, Journal of Materials; 57(1): 72-79, 2005.

Appendix A: Test Protocols

HITF08282

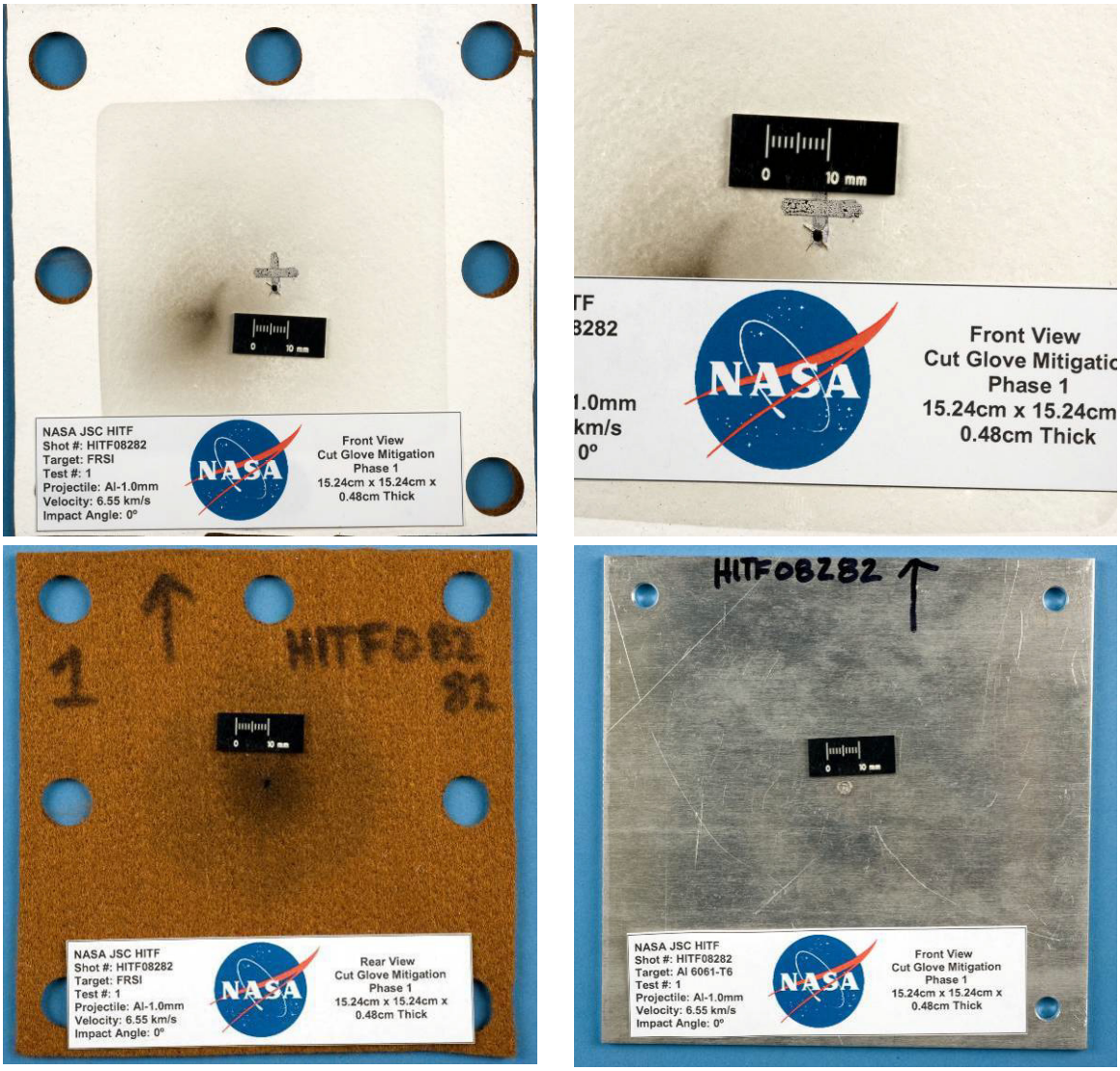

Figure 1: HITF08282 post-test damage photographs. Top left to bottom right: overwrap front side, overwrap front side (zoom), overwrap rear side, target plate front side.

Test #1 of Phase 1 (HITF08282) investigated a 1.0 mm diameter Al 2017-T4 sphere impacting at a velocity of 6.55 km/s with normal incidence (0°) on a 4.826mm thick Al6061-T6 plate covered by a Felt Reusable Surface Insulation (FRSI) overwrap. Impact of the projectile generated a roughly circular entry hole in the overwrap, with four radial cracks (length ≈ 3mm) propagating from each corner of the hole. On the rear side, the exit hole was centered in a zone of dark discoloration (diameter ≈ 19mm). The crater on the target plate was clearly formed with a roughly hemispherical shape and a protruding crater lip. There was no noticeable damage on the rear side of the target.

Overwrap						
Front					Rear	
$d_{h,1}$ (mm)	$d_{h,2}$ (mm)	L_c (mm)	$D_{max,1}$ (mm)	$D_{max,2}$ (mm)	$d_{h,1}$ (mm)	$d_{h,2}$ (mm)
1.7	1.7	3.0	5.1	4.5	3.0	3.0

Target							
Front					Rear		
$d_{c,1}$ (mm)	$d_{c,2}$ (mm)	l_{max} (mm)	p_{max} (mm)	V_c (mm^3)	b_{max} (mm)	$D_{max,1}$ (mm)	$D_{max,2}$ (mm)
3.4	3.4	0.3	1.2	4.6	0	0	0

Table 1: Phase 1 test #1, HITF08282 (FRSI overwrap) target damage measurements.

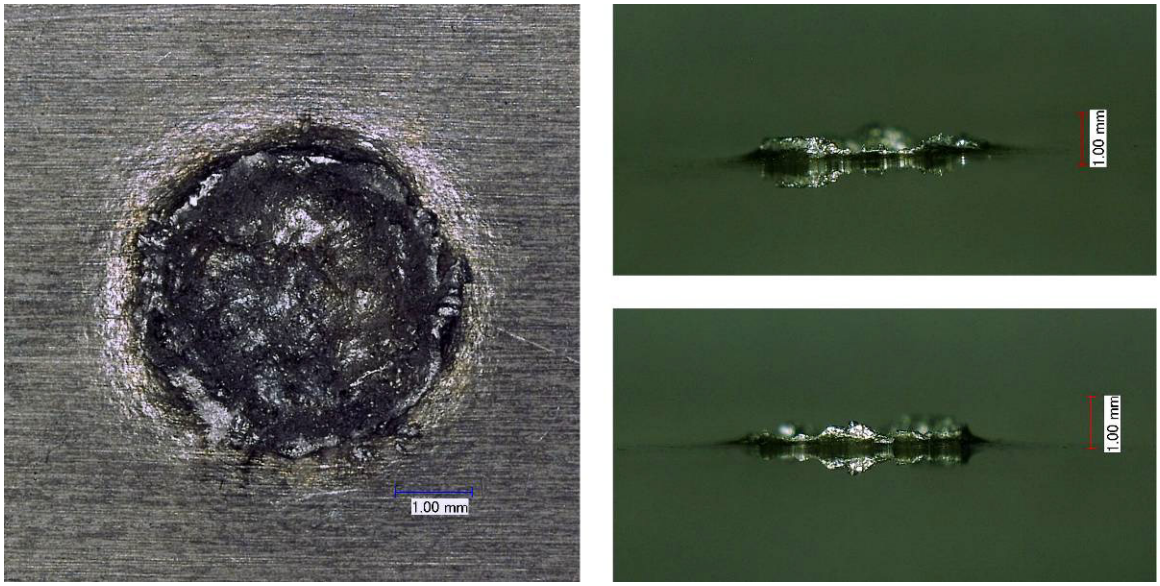

Figure 2: HITF08282 impact crater.

HITF08242

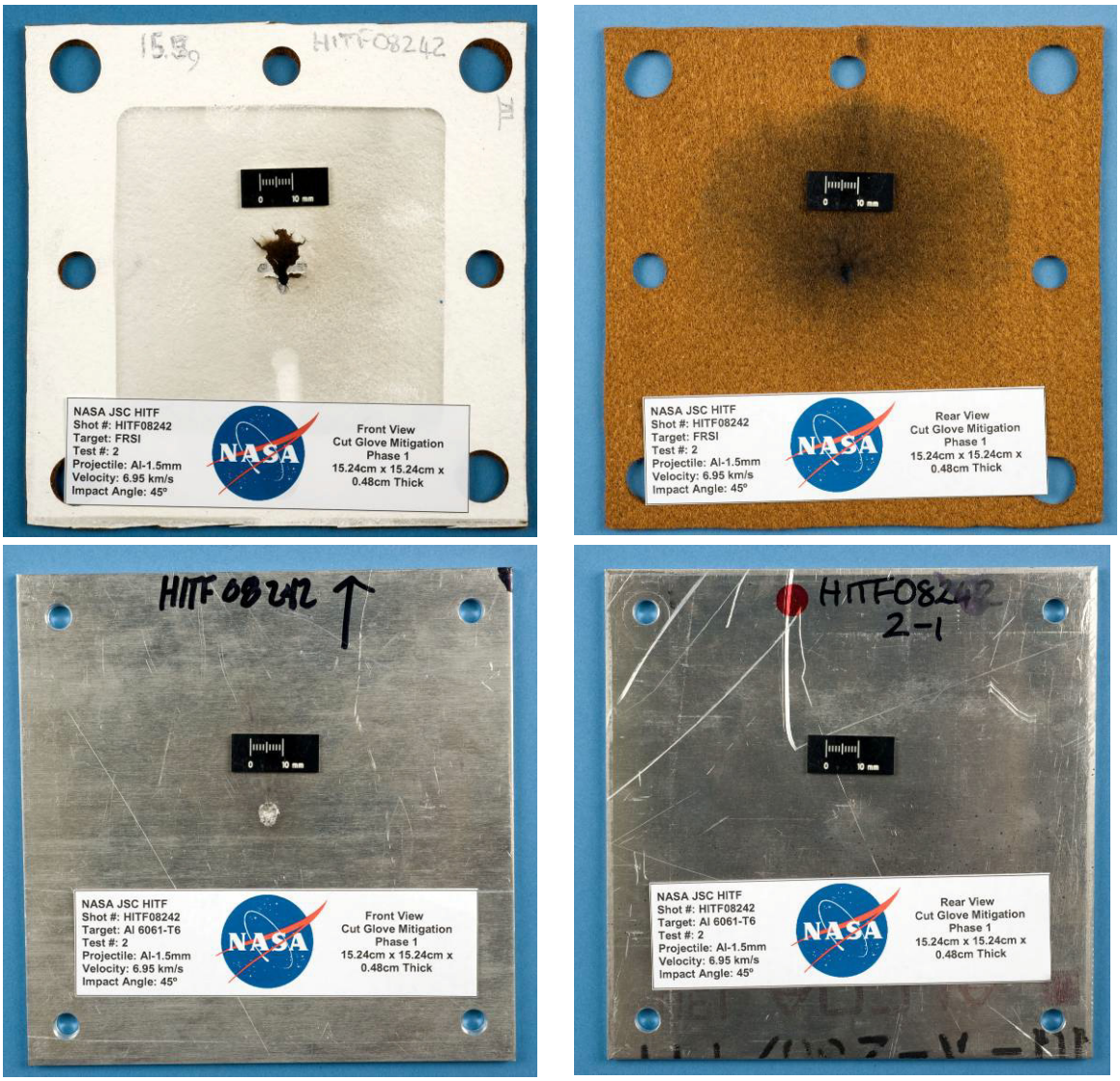

Figure 3: HITF08242 post-test damage photographs. Top left to bottom right: overwrap front side, overwrap rear side, target plate front side, target plate rear side.

Test #2 of Phase 1 (HITF08242) investigated a 1.5 mm diameter Al 2017-T4 sphere impacting obliquely (45°) with a velocity of 6.95 km/s on a 4.826 mm thick Al6061-T6 plate covered by a FRSI overwrap. Impact of the projectile generated an elliptical entry hole in the overwrap, which was surrounded by a number of cracks (~8) and frayed felt. The rear side of the overwrap showed a semi circular region of discoloration (radius ≈ 52mm) about the elliptical exit hole, with the darkest region located above the clear hole. The crater on the target plate was clearly formed, slightly elliptical in shape with a sharply protruding crater lip (max height = 0.7 mm). The rear side of the target showed a minimal amount of bulging.

Overwrap						
Front					Rear	
$d_{h,1}$ (mm)	$d_{h,2}$ (mm)	L_c (mm)	$D_{max,1}$ (mm)	$D_{max,2}$ (mm)	$d_{h,1}$ (mm)	$d_{h,2}$ (mm)
6.4	18.3	13.4	16.8	20.3	4.2	8.9

Target							
Front					Rear		
$d_{c,1}$ (mm)	$d_{c,2}$ (mm)	l_{max} (mm)	p_{max} (mm)	V_c (mm^3)	b_{max} (mm)	$D_{max,1}$ (mm)	$D_{max,2}$ (mm)
4.7	6.5	0.7	1.2	12.1	0.1	6.4	7.8

Table 2: Phase 1 test #2, HITF08242 (FRSI overwrap) target damage measurements.

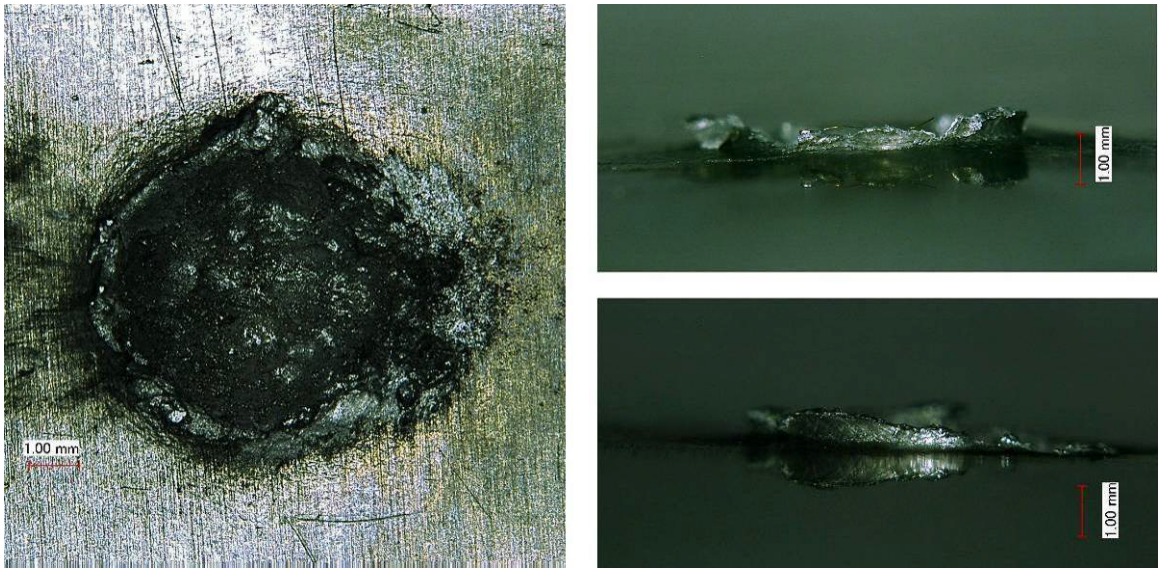

Figure 4: HITF08242 impact crater.

HITF08283

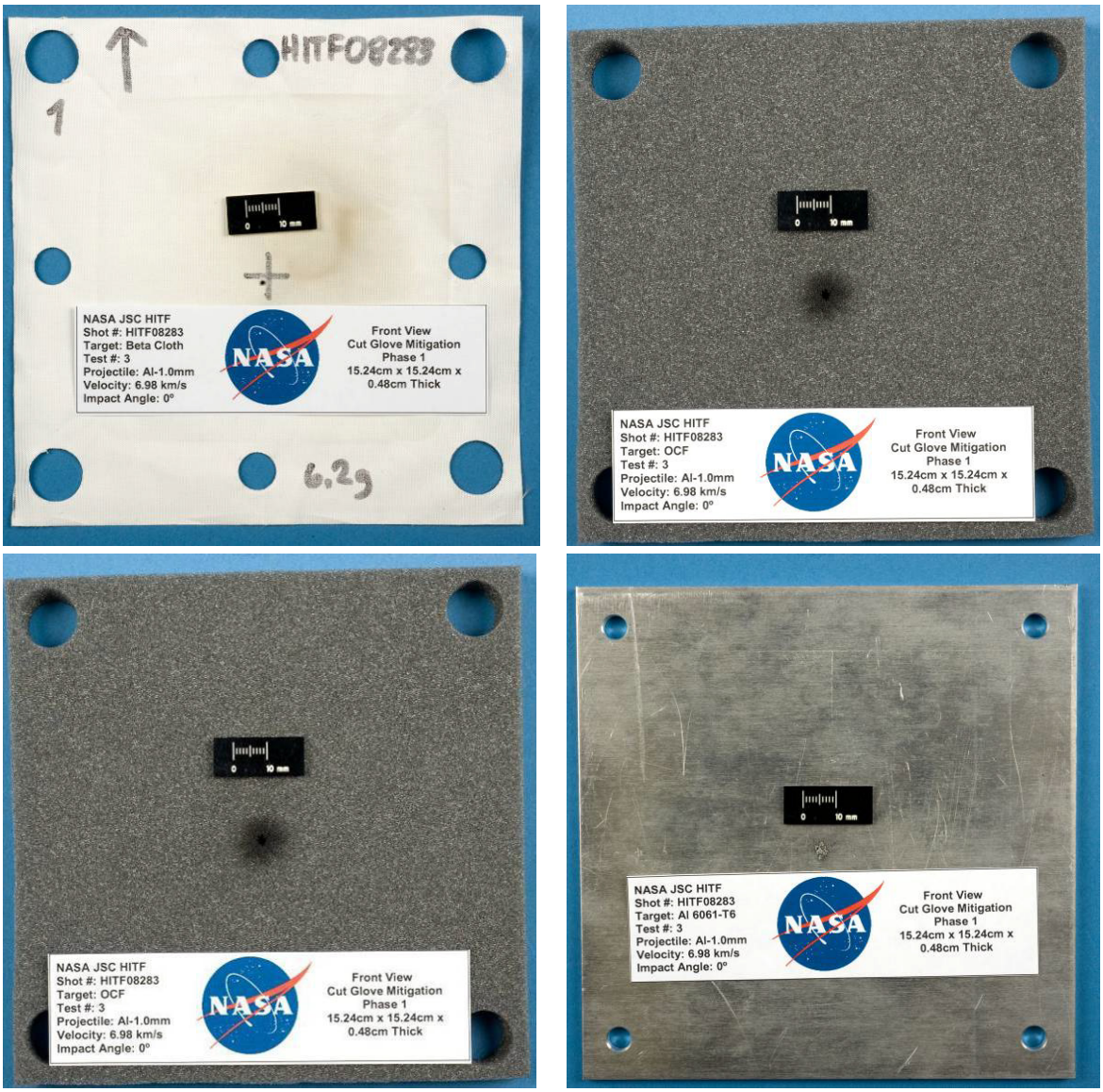

Figure 5: HITF08283 post-test damage photographs. Top left to bottom right: beta-cloth cover front side, open cell foam front side, open cell foam rear side, target plate rear side.

Test #3 of Phase 1 (HITF08283) investigated a 1.0 mm diameter Al 2017-T4 sphere impacting at a velocity of 6.98 km/s with normal incidence (0°) on a 4.826mm thick Al6061-T6 plate covered by a non-*reticulated* open cell polyether polyurethane foam (OCF) with an aluminized beta-cloth cover. Impact of the projectile generated a circular entry hole in the beta cloth. The OCF shows a roughly circular through hole with surrounding black discoloration. The exit hole in the OCF is larger than the entry hole, suggesting an expanding fragment cloud. The target plate shows a single large crater, with numerous smaller craters and melted aluminum deposits about the central damage zone. The large crater is circular shape with a small lip height. There is no noticeable damage on the rear side of the target plate.

Overwrap							
Beta Cloth		Foam					
		Front				Rear	
$d_{h,1}$ (mm)	$d_{h,2}$ (mm)	$d_{h,1}$ (mm)	$d_{h,2}$ (mm)	$D_{max,1}$ (mm)	$D_{max,2}$ (mm)	$d_{h,1}$ (mm)	$d_{h,2}$ (mm)
2.6	3.6	3.0	3.0	8.0	8.0	8.5	7.2

Target							
Front					Rear		
$d_{c,1}$ (mm)	$d_{c,2}$ (mm)	l_{max} (mm)	p_{max} (mm)	V_c (mm^3)	$b,_{max}$ (mm)	$D_{max,1}$ (mm)	$D_{max,2}$ (mm)
1.1	1.3	0.1	0.9	0.9	0	0	0

Table 3: Phase 1 test #3, HITF08283 (OCF+BC overwrap) target damage measurements.

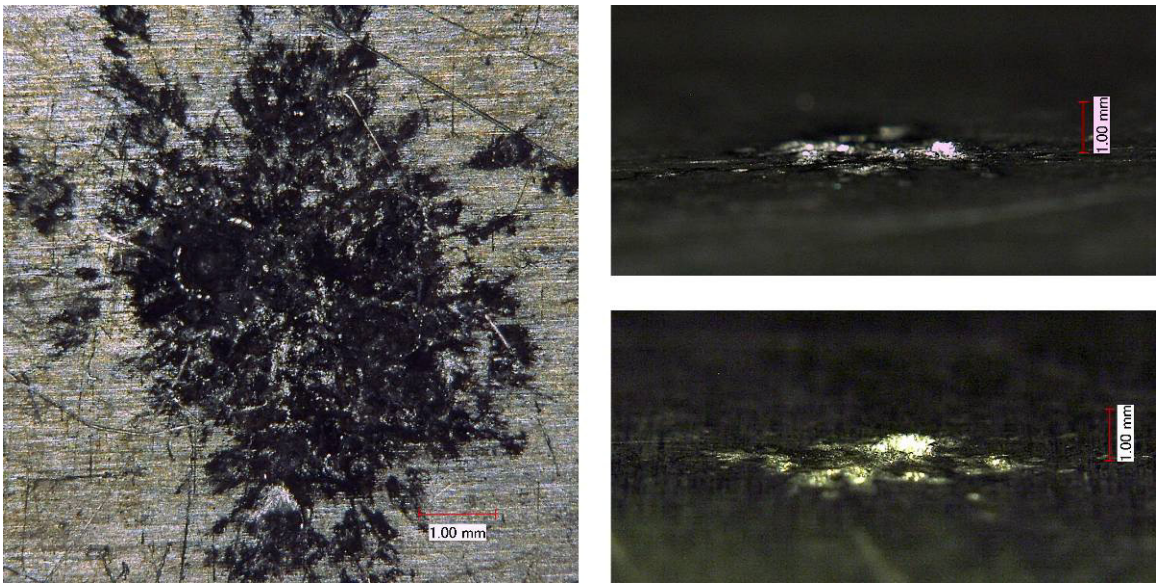

Figure 6: HITF08283 impact crater.

HITF08243

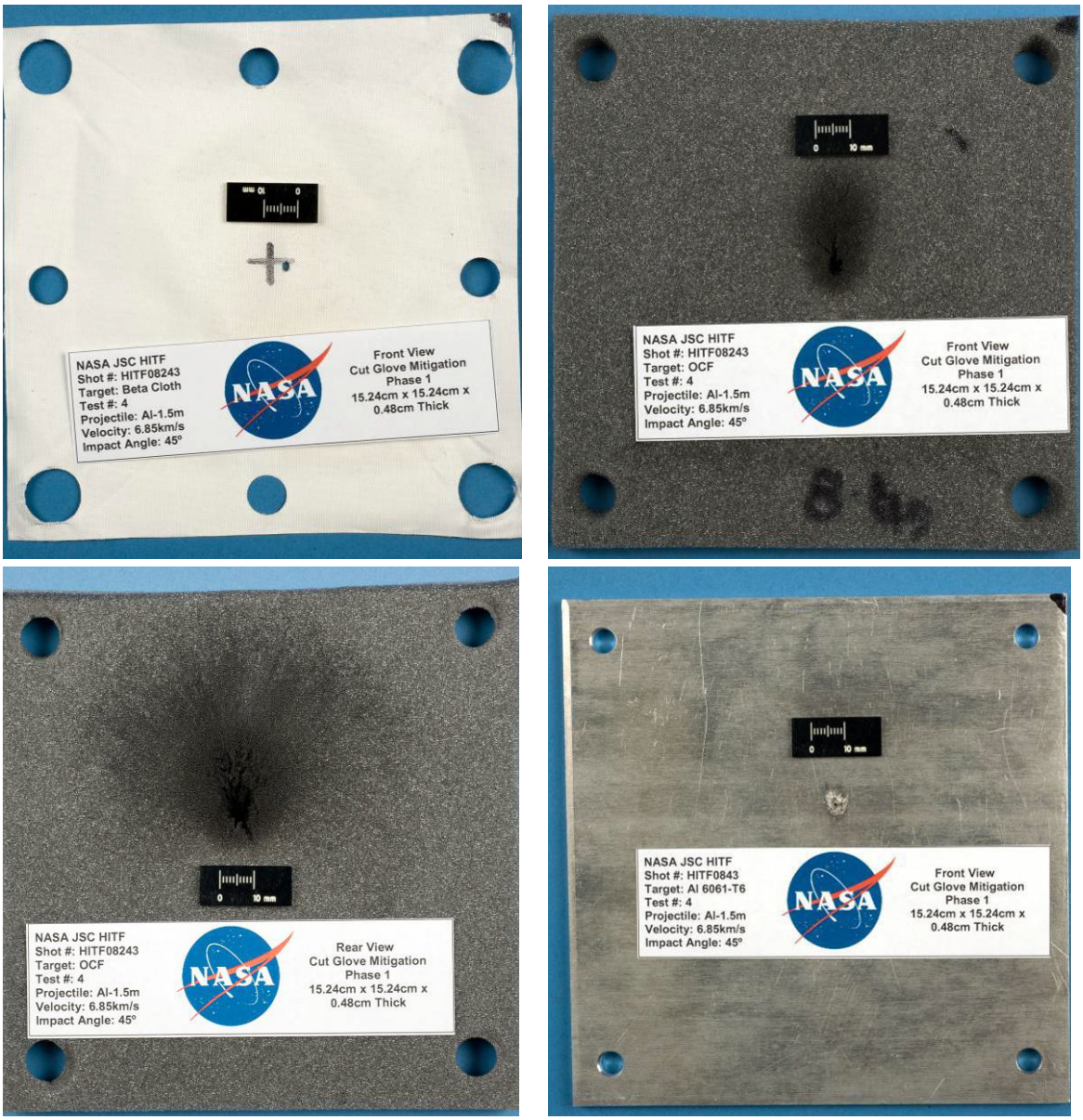

Figure 7: HITF08243 post-test damage photographs. Top left to bottom right: beta cloth cover front side, open cell foam front side, open cell foam rear side, target plate front side.

Test #4 of Phase 1 (HITF08243) investigated a 1.5 mm diameter Al 2017-T4 sphere impacting obliquely (45°) with a velocity of 6.95 km/s on a 4.826 mm thick Al6061-T6 plate covered by a non-reticulated open cell polyether polyurethane foam (OCF) with an aluminized beta-cloth cover. Impact of the projectile generated an elliptical entry hole in the beta cloth. The entry hole in the OCF is elliptical in shape with a diameter larger than that of the clear hole in the beta-cloth. The exit hole diameter in the OCF is larger than the entry hole, suggesting an expanding fragment cloud. The foam about the clear hole is discolored (black). The target plate shows multiple overlapping craters, creating a single roughly elliptical-shaped crater. There are melted deposits of aluminum at the bottom of the craters as well and black striations on the plate above the cratered area. There is no apparent damage to the rear side of the target plate.

Overwrap							
Beta Cloth		Foam					
		Front				Rear	
$d_{h,1}$ (mm)	$d_{h,2}$ (mm)	$d_{h,1}$ (mm)	$d_{h,2}$ (mm)	$D_{max,1}$ (mm)	$D_{max,2}$ (mm)	$d_{h,1}$ (mm)	$d_{h,2}$ (mm)
5.7	9.7	4.5	14.1	8.0	8.0	10.5	20.5

Target							
		Front			Rear		
$d_{c,1}$ (mm)	$d_{c,2}$ (mm)	l_{max} (mm)	p_{max} (mm)	V_c (mm^3)	$b,_{max}$ (mm)	$D_{max,1}$ (mm)	$D_{max,2}$ (mm)
3.1	3.1	0.3	1.5	1.8	0	0	0

Table 4: Phase 1 test #4, HITF08243 (OCF+BC overwrap) target damage measurements.

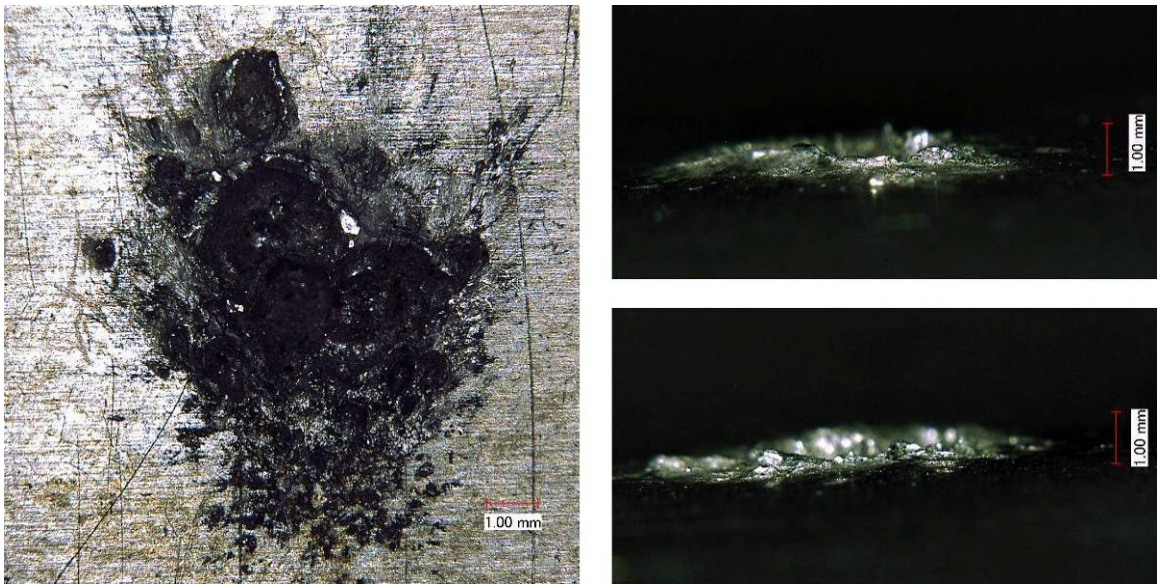

Figure 8: HITF08243 impact crater.

HITF08284

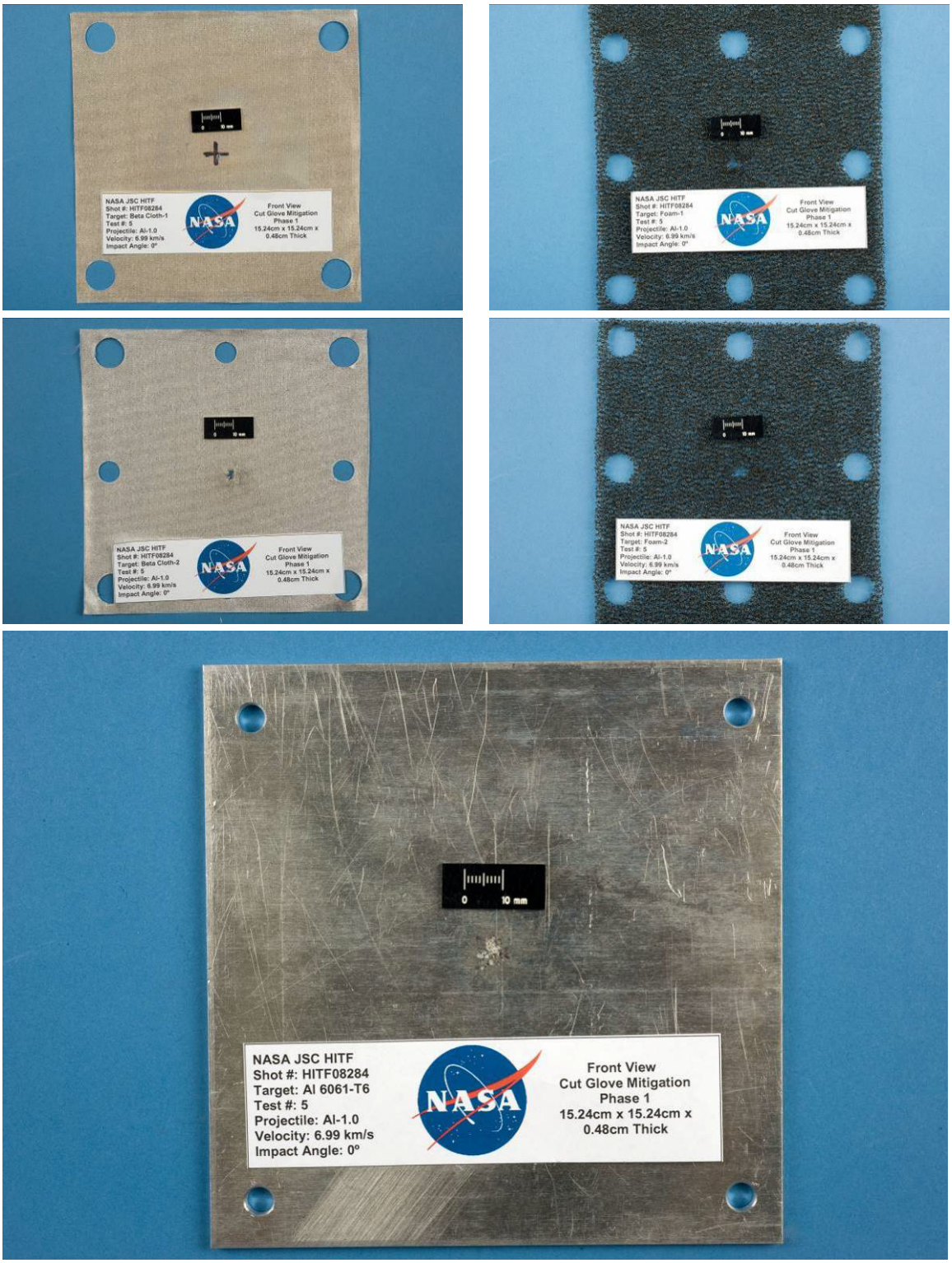

Figure 9: HITF08284 post-test damage photographs. Top to bottom: outer beta-cloth cover front side (left), outer open cell foam layer front side (right), inner beta-cloth cover (left), inner open cell foam layer (right), target plate front side.

Test #5 of Phase 1 (HITF08284) investigated a 1.0 mm diameter Al 2017-T4 sphere impacting at a velocity of 6.98 km/s with normal incidence (0°) on a 4.826mm thick Al6061-T6 plate covered by a double-layer open-cell polyurethane foam overwrap with beta-cloth cover and intermediate layer (DROCF + BC). Impact of the projectile on the overwrap generated a roughly circular entry hole, which was slightly frayed about the edges. The evolution of hole size through both layers of the ROCF and intermediate beta-cloth layer show an expanding fragment cloud (i.e. progressively larger hole diameters). There is minimal damage on the target plate, consisting of some black discoloration and a single shallow crater showing the projectile barely perforating the surface of the target plate. There is no apparent damage to the rear side of the target plate.

Overwrap							
BC-1		*Foam-1 Front*		*BC-2*		*Foam-2 Front*	
$d_{h,1}$ *(mm)*	$d_{h,2}$ *(mm)*	$d_{h,1}$ *(mm)*	$d_{h,2}$ *(mm)*	$d_{h,1}$ *(mm)*	$d_{h,2}$ *(mm)*	$d_{h,1}$ *(mm)*	$d_{h,2}$ *(mm)*
1.32	1.32	3.68	4.28	3.46	5.04	4.43	4.86

Target Front				
$d_{h,1}$ *(mm)*	$d_{h,2}$ *(mm)*	l_{max} *(mm)*	p_{max} *(mm)*	V_c *(mm^3)*
1.0	1.0	0.1	0.1	<0.1

Table 5: Phase 1 test #5, HITF08284 (DROCF+BC overwrap) target damage measurements.

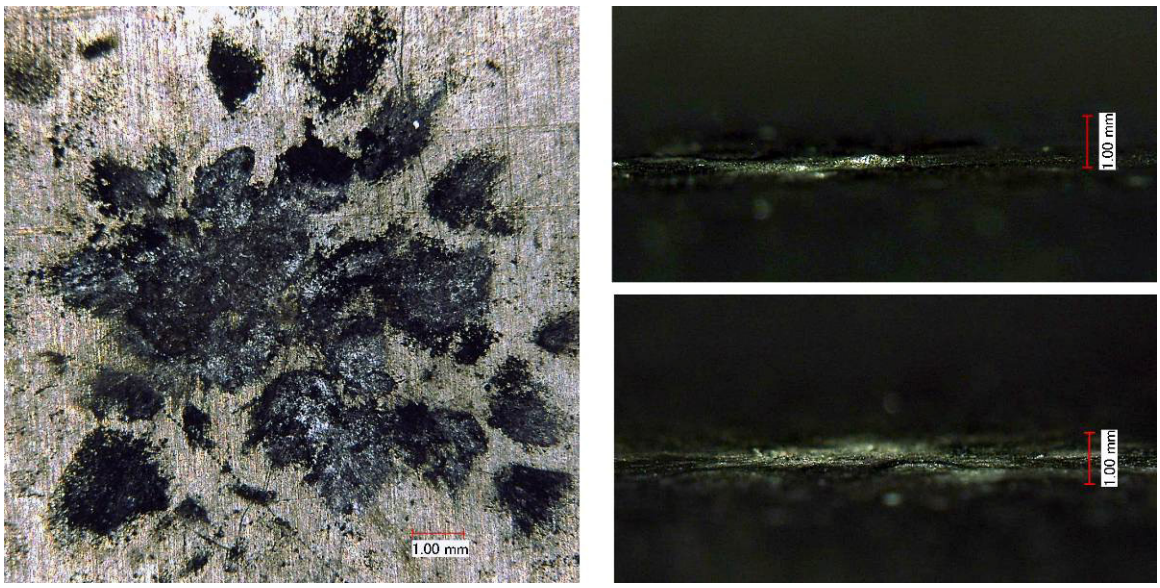

Figure 10: HITF08284 impact crater.

HITF08244

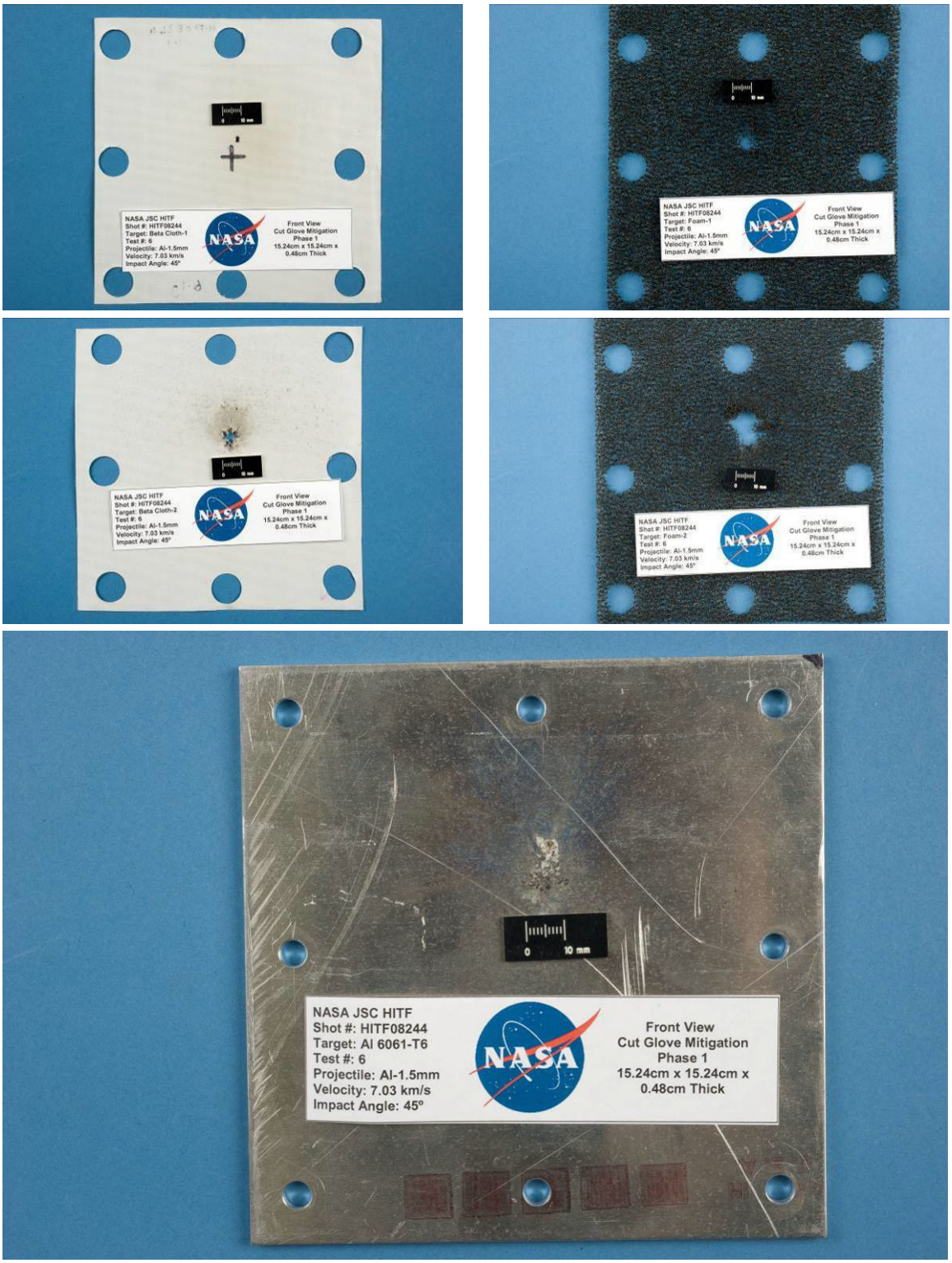

Figure 11: HITF08244 post-test damage photographs. Top to bottom: outer beta-cloth cover front side (left), outer open cell foam layer front side (right), inner beta-cloth cover (left), inner open cell foam layer (right), target plate front side.

Test #6 of Phase 1 (HITF08244) investigated a 1.5 mm diameter Al 2017-T4 sphere impacting obliquely (45°) with a velocity of 7.03 km/s on a 4.826 mm thick Al6061-T6 plate covered by a double-layer open-cell polyurethane foam overwrap with beta-cloth cover and intermediate layer (DROCF + BC). Impact of the projectile generated an elliptical entry hole in the beta cloth. The clear hole diameter increases with progression through the overwrap layers, suggesting an expanding fragment cloud. There is a single elliptical-shaped crater on the front side of the target plate with black discoloration and melted aluminum deposits below the crater.

Overwrap							
BC-1		*Foam-1 Front*		*BC-2*		*Foam-2 Front*	
$d_{h,1}$ *(mm)*	$d_{h,2}$ *(mm)*	$d_{h,1}$ *(mm)*	$d_{h,2}$ *(mm)*	$d_{h,1}$ *(mm)*	$d_{h,2}$ *(mm)*	$d_{h,1}$ *(mm)*	$d_{h,2}$ *(mm)*
1.98	3.30	11.46	16.3	8.8	11.6	17.4	22.5

Target Front				
$d_{h,1}$ *(mm)*	$d_{h,2}$ *(mm)*	l_{max} *(mm)*	p_{max} *(mm)*	V_c *(mm^3)*
2.32	2.48	0.8	1.4	2.00

Table 6: Phase 1 test #6, HITF08244 (DROCF+BC overwrap) target damage measurements.

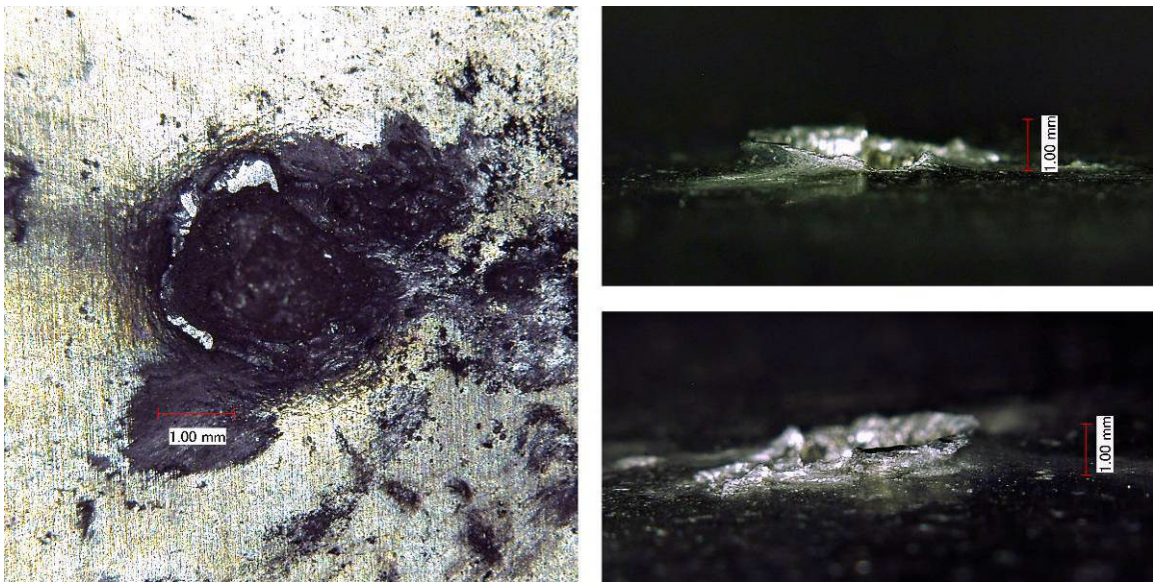

Figure 12: HITF08244 impact crater.

HITF08250

Figure 13: HITF08250 post-test damage photographs. Clockwise from top left: outer beta-cloth cover front side, innermost beta-cloth cover rear side, target plate front side.

Test #7 of Phase 1 (HITF08250) investigated a 1.0 mm diameter Al 2017-T4 sphere impacting at a velocity of 6.86 km/s with normal incidence on a 4.826 mm thick Al6061-T6 plate covered by an overwrap consisting of 16 layers of 20 micron thick aluminized beta-cloth, separated by Dacron netting spacers (commonly used in MLI). Impact of the projectile generated a roughly circular entry hole in the overwrap. The rear side of the beta-cloth overwrap shows a small bulge (diameter ≈ 5 mm) with a single vertical tear through its center. There is a small amount of discoloration (black) of the target plate, which is likely deposits of charred beta-

cloth fibers. There is no noticeable damage to the target surface (i.e. craters, protrusions, etc.) or target rear side.

Overwrap						
Front					Rear	
$d_{h,1}$ (mm)	$d_{h,2}$ (mm)	L_c (mm)	$D_{max,1}$ (mm)	$D_{max,2}$ (mm)	$d_{h,1}$ (mm)	$d_{h,2}$ (mm)
2.15	2.24	11.6	3.30	3.69	4.3	5.4

Target							
Front						Rear	
d_{c1} (mm)	d_{c2} (mm)	l_{max} (mm)	p_{max} (mm)	V_c (mm^3)	b_{max} (mm)	$D_{max,1}$ (mm)	$D_{max,2}$ (mm)
<0.1	<0.1	0	0	0	0	0	0

Table 7: Phase 1 test #7, HITF08250 (DROCF+BC overwrap) target damage measurements.

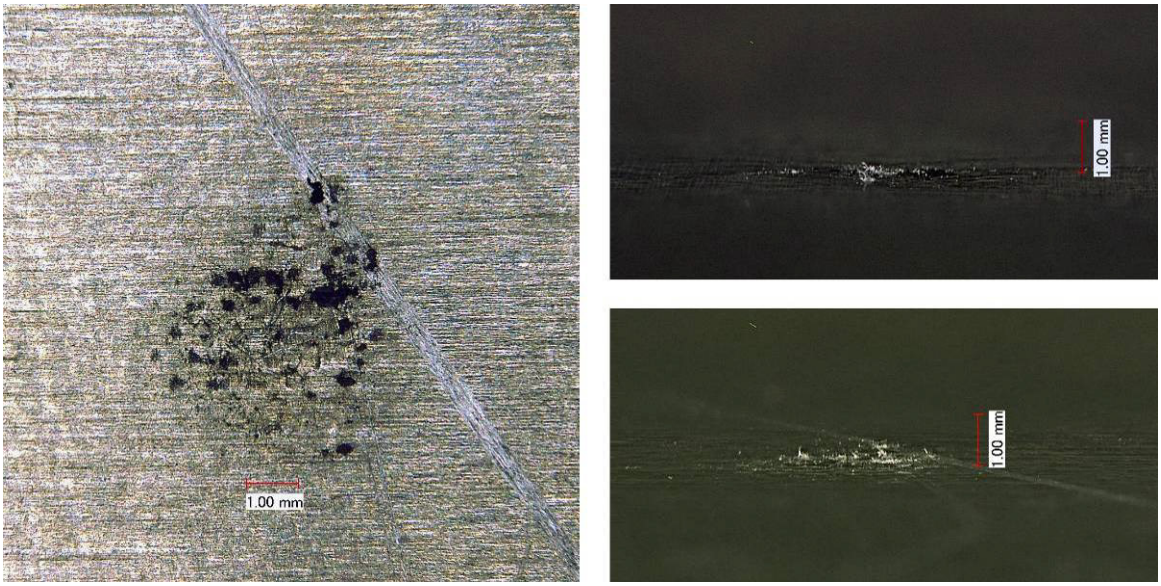

Figure 14: HITF08250 impact crater.

HITF08245

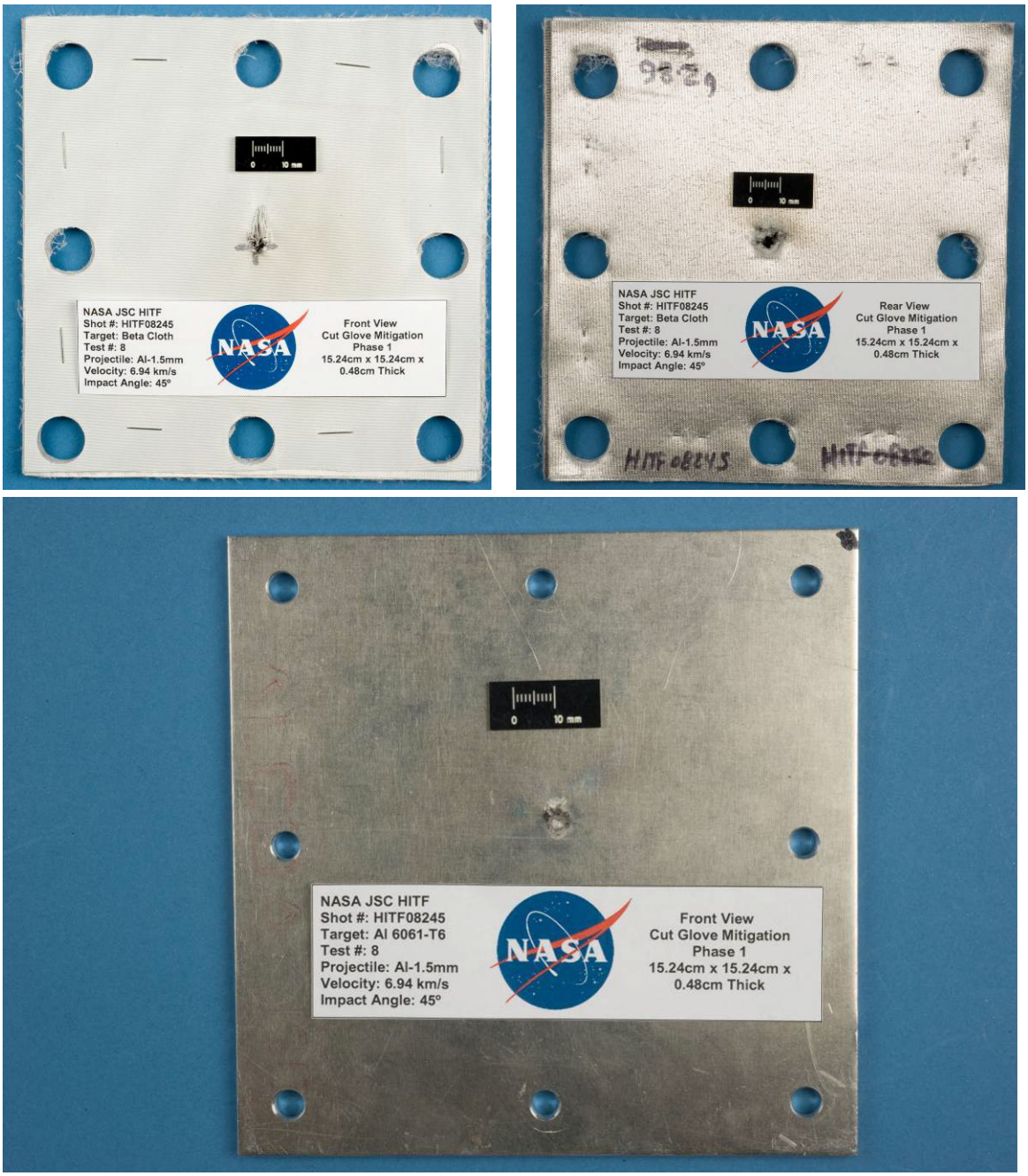

Figure 15: HITF08245 post-test damage photographs. Clockwise from top left: outer beta-cloth cover front side, innermost beta-cloth cover rear side, target plate front side.

Test #8 of Phase 1 (HITF08245) investigated a 1.5 mm diameter Al 2017-T4 sphere impacting obliquely (45°) with a velocity of 6.94 km/s on a 4.826 mm thick Al6061-T6 plate covered by an overwrap consisting of 16 layers of 20 micron thick aluminized beta-cloth, separated by Dacron netting spacers (commonly used in MLI). Impact of the projectile generated a roughly circular entry hole in the overwrap, with a single tear (length ≈ 12mm) above the hole. The exit hole in the overwrap is considerably larger than the entry hole,

suggesting a fragmented projectile and expanding fragment cloud. The target plate showed a circular pattern of melted aluminized beta cloth with black discoloration above it.

Overwrap						
Front					Rear	
$d_{h,1}$ (mm)	$d_{h,2}$ (mm)	L_c (mm)	$D_{max,1}$ (mm)	$D_{max,2}$ (mm)	$d_{h,1}$ (mm)	$d_{h,2}$ (mm)
2.15	5.26	12.2	8.76	17.66	4.08	4.57

Target							
Front						Rear	
d_{c1} (mm)	d_{c2} (mm)	l_{max} (mm)	p_{max} (mm)	V_c (mm^3)	b_{max} (mm)	$D_{max,1}$ (mm)	$D_{max,2}$ (mm)
<0.1	<0.1	0	0	0	0	0	0

Table 8: Phase 1 test #8, HITF08245 (DROCF+BC overwrap) target damage measurements.

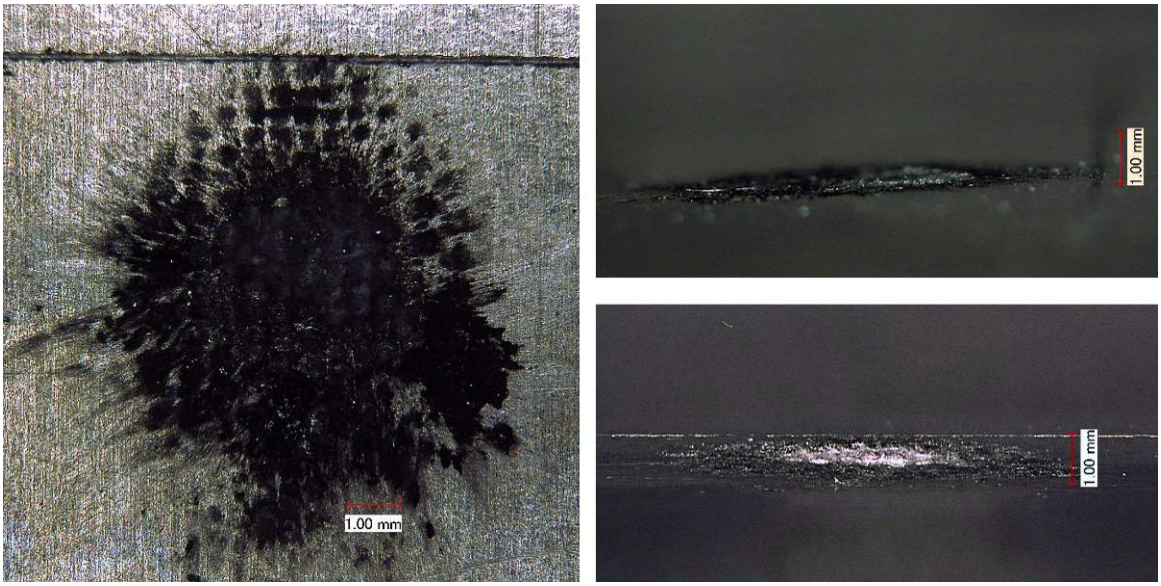

Figure 16: HITF08245 impact crater.

HITF08247

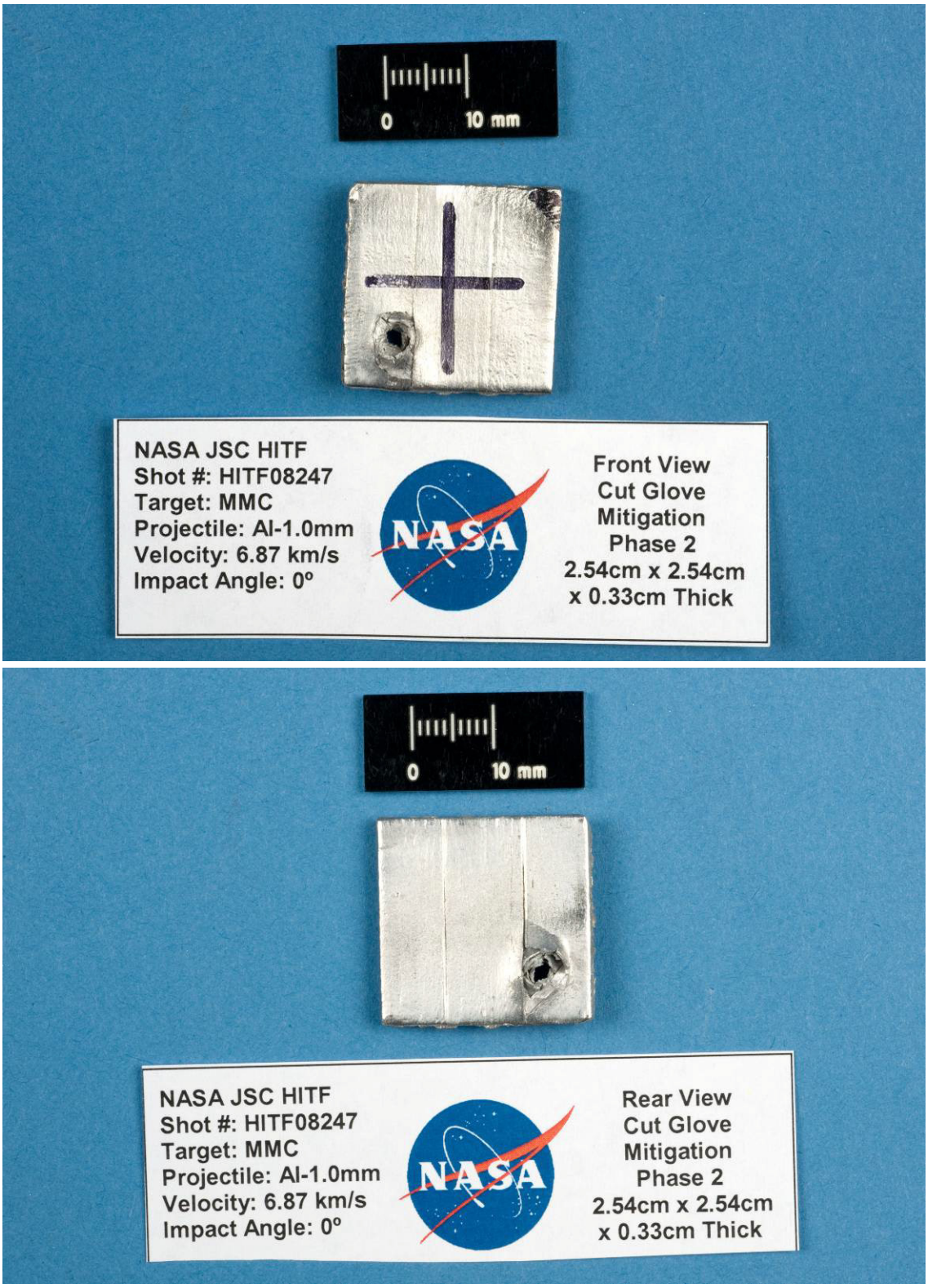

Figure 17: HITF08247 post-test damage photographs. Top to bottom: front side damage (entry hole), rear side damage (exit hole).

Test #1 of Phase 2 (HITF08247) investigated a 1.0 mm diameter Al 2017-T4 sphere impacting at a velocity of 6.87 km/s with normal incidence (0°) on a 3.3mm thick Nextel 610 fiber reinforced aluminum composite. The projectile clearly perforated the target, generating a circular entry hole. The upper lamina of the MMC shows brittle failure of the crater lip, resulting in the maximum lip height being measured on the 2nd composite lamina. The rear of target shows an elliptical clear hole with surface spallation of the outer ply. There is some cracking on the top edge of exit hole as well as some slight petalling about the lower edge of the hole.

Front							*Rear*		
$d_{c,1}$ *(mm)*	$d_{c,2}$ *(mm)*	$D_{max,1}$ *(mm)*	$D_{max,2}$ *(mm)*	l_{max} *(mm)*	p_{max} *(mm)*	V_c *(mm^3)*	$d_{h,1}$ *(mm)*	$d_{h,2}$ *(mm)*	b_{max} *(mm)*
4.3	3.04	5.63	5.38	1.00	N/A	N/A	11.3	7.73	2.45

Table 9: Phase 2 test #1, HITF08247 Nextel 610/pure Al MMC target damage measurements.

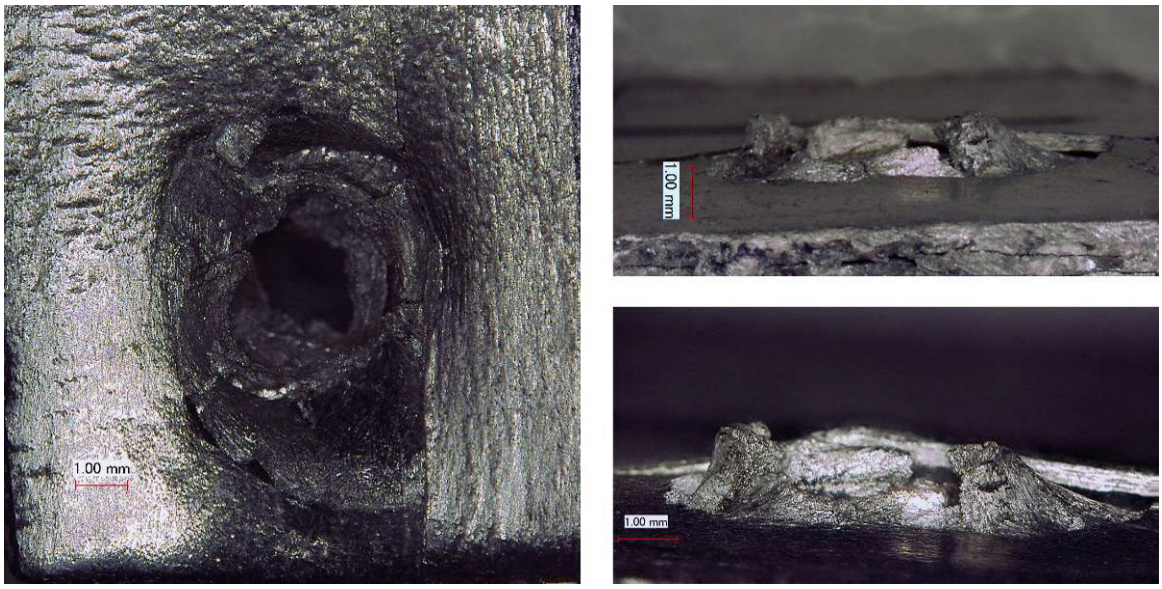

Figure 18: HITF08247 impact crater.

HITF08248

Figure 19: HITF08248 post-test damage photographs. Top to bottom: front side damage (entry hole), rear side damage (surface spallation).

Test #2 of Phase 2 (HITF08248) investigated a 1.0 mm diameter Al 2017-T4 sphere impacting at a velocity of 6.91 km/s with normal incidence on a 7.03 mm thick CFRP panel. Impact from the projectile generated a circular entry hole with significant surface spallation and cracking along the target vertical axis. Although the entry hole does not have any visible lip, the spalled fibers protrude significantly from the face of the laminate. An area (≈ 4mm x 14mm) of adhesive (AF191) was spalled from the rear side of the target, however this is not considered as damage to the test article as the CFRP rear side was undamaged.

Front							*Rear*		
$d_{c,1}$ *(mm)*	$d_{c,2}$ *(mm)*	$D_{max,1}$ *(mm)*	$D_{max,2}$ *(mm)*	l_{max} *(mm)*	p_{max} *(mm)*	V_c *(mm^3)*	$d_{b,1}$ *(mm)*	$d_{b,2}$ *(mm)*	b_{max} *(mm)*
2.1	2.1	5.2	79.6	0	2.7	0.9	N/A	N/A	N/A

Table 10: Phase 2 test #2, HITF08248 CFRP target damage measurements.

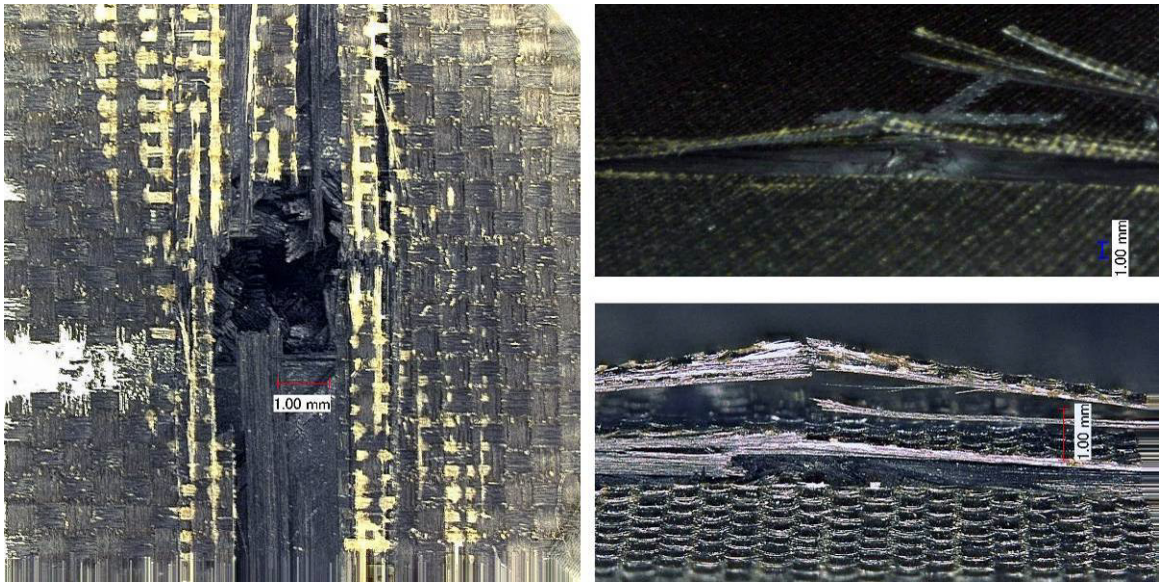

Figure 20: HITF08248 impact crater.

HITF08249

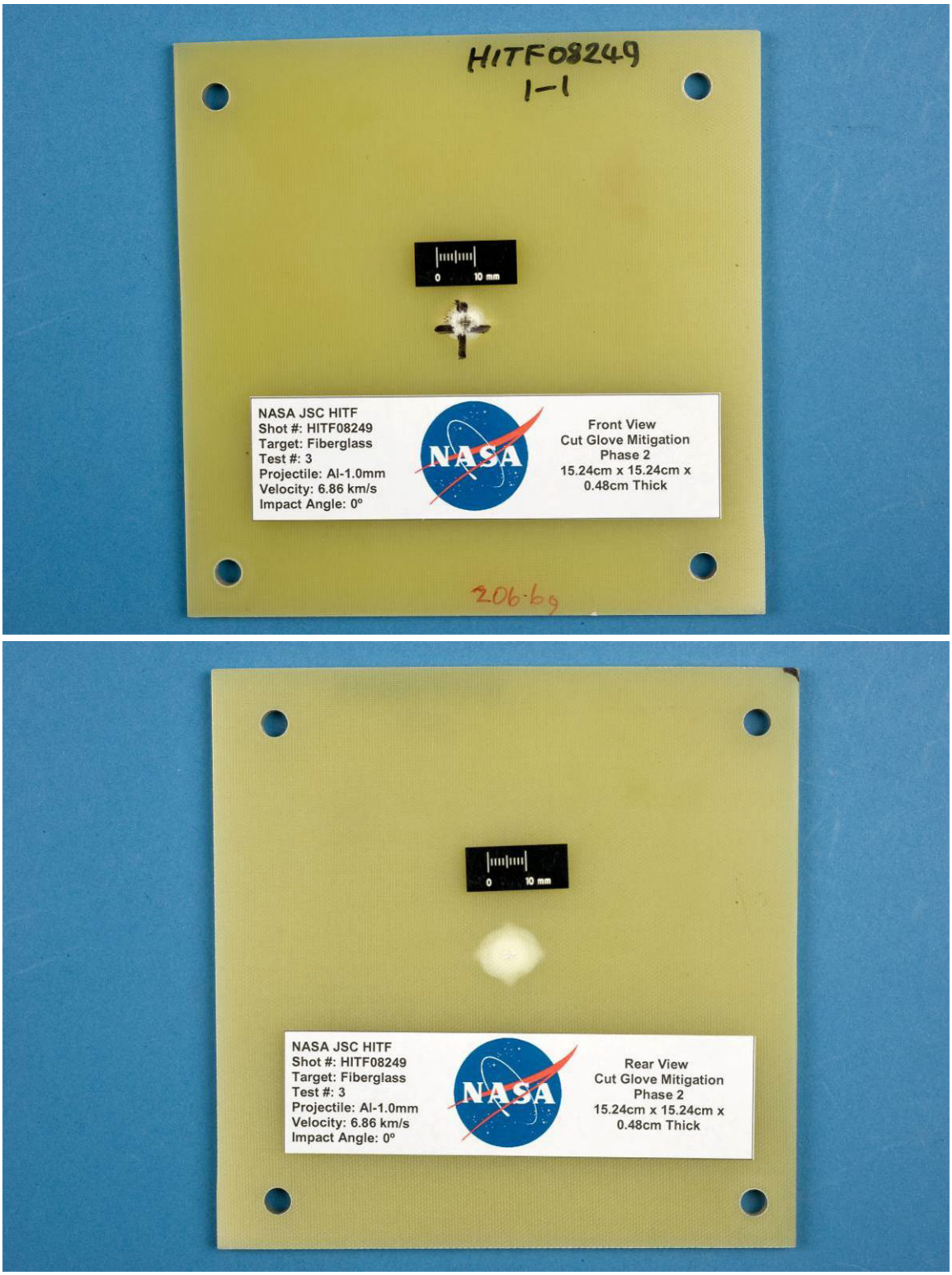

Figure 21: HITF08249 post-test damage photographs. Top to bottom: front side damage (entry hole), rear side damage (white area is internal damage and delamination).

Test #3 of Phase 2 (HITF08249) investigated a 1.0 mm diameter Al 2017-T4 sphere impacting at a velocity of 6.86 km/s with normal incidence (0°) on a 4.826mm thick NP500CR fiberglass composite panel. There is a roughly circular entry hole, about which frayed and broken glass fibers are observable. There is clear internal delamination, identified as a white area about the clear hole, which measures ~11mm in diameter. The rear of target shows a small area of surface damage (considerably smaller than the extent of internal delamination), which is slightly bulged from the plane of the target rear side. There is noticeable bias of the delamination along the fiberglass primary in-plane directions.

Front							*Rear*		
$d_{c,1}$ (mm)	$d_{c,2}$ (mm)	$D_{max,1}$ (mm)	$D_{max,2}$ (mm)	l_{max} (mm)	p_{max} (mm)	V_c (mm^3)	$d_{b,1}$ (mm)	$d_{b,2}$ (mm)	b_{max} (mm)
2.6	2.6	7.6	7.6	0.8	0.6	0.6	6.2	6.2	0.3

Table 11: Phase 2 test #3, HITF08249 fiberglass target damage measurements.

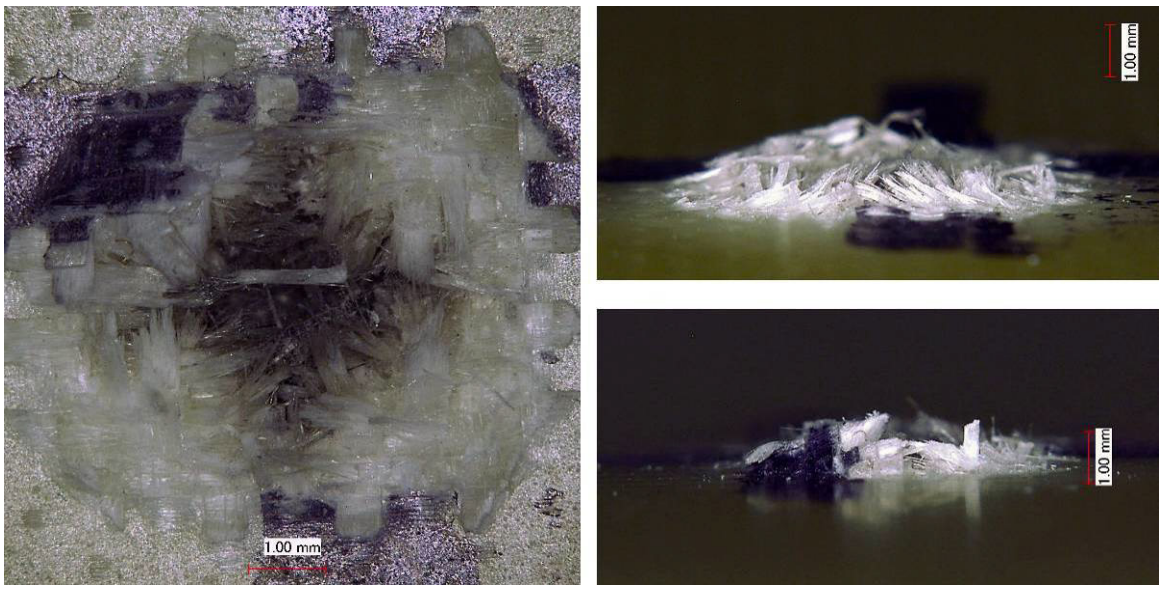

Figure 22: HITF08249 impact crater.

HITF08330

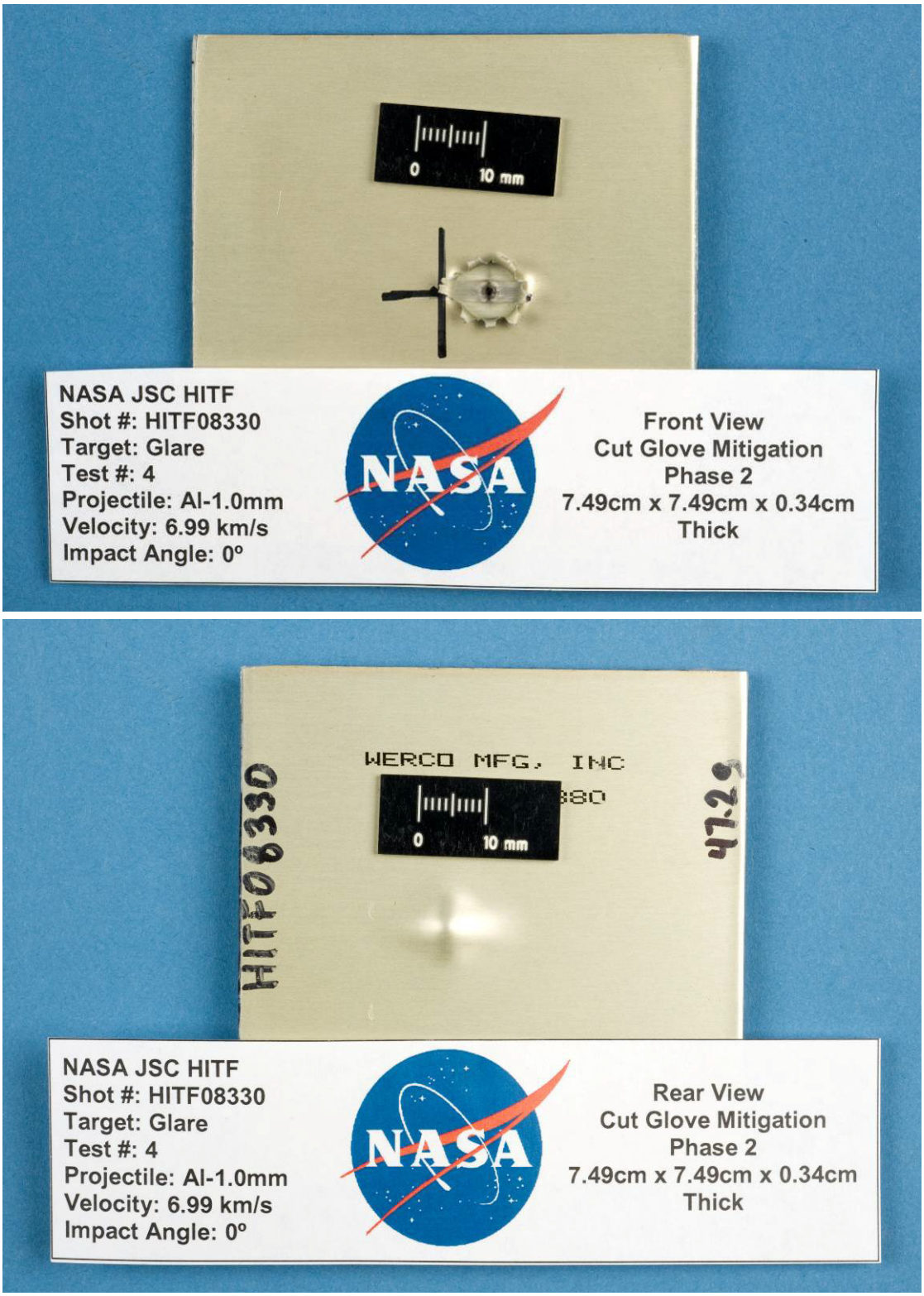

Figure 23: HITF08330 post-test damage photographs. Top to bottom: front side damage (entry hole), rear side damage (rear surface bulge).

Test #4 of Phase 2 (HITF08330) investigated a 1.0 mm diameter Al 2017-T4 sphere impacting at a velocity of 6.99 km/s with normal incidence (0°) on a 3.4mm thick glass-reinforced Fiber Metal Laminate (Glare). Impact from the projectile generated an entry hole into the target which was circular in shape with petalling of the crater lip (seven petals, height = 3.5mm). The petals are formed from the upper aluminum layer in the FML. The rear of target shows a steep bulge, however there is no spallation of any material.

Front							*Rear*		
$d_{c,1}$ *(mm)*	$d_{c,2}$ *(mm)*	$D_{max,1}$ *(mm)*	$D_{max,2}$ *(mm)*	l_{max} *(mm)*	p_{max} *(mm)*	V_c *(mm^3)*	$d_{b,1}$ *(mm)*	$d_{b,2}$ *(mm)*	b_{max} *(mm)*
8.3	9.7	10.8	12.5	3.5	0.3	0.1	10.0	10.0	1.69

Table 12: Phase 2 test #4, HITF08330 GLARE FML target damage measurements.

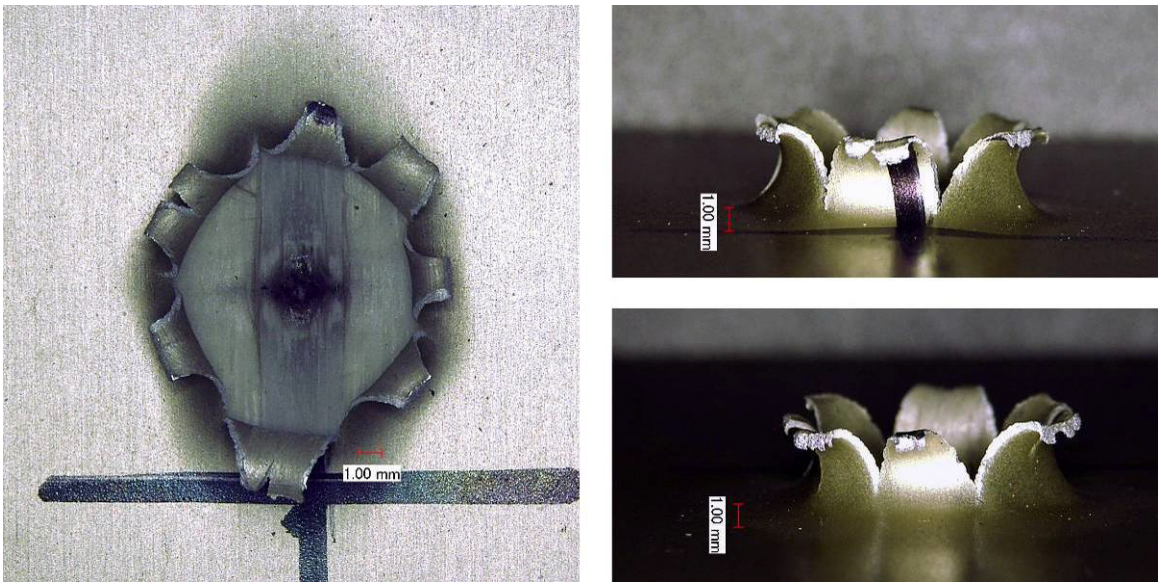

Figure 24: HITF08330 impact crater.